San Jose State University

SJSU ScholarWorks

Spring 2014

Plankton in Monterey Bay: Optimization of Optical Sensor Data from Autonomous Underwater Vehicles with Applications in Plankton Community Composition

Diane Wyse
San Jose State University

PLANKTON IN MONTEREY BAY:
OPTIMIZATION OF OPTICAL SENSOR DATA FROM AUTONOMOUS
UNDERWATER VEHICLES WITH APPLICATIONS IN PLANKTON COMMUNITY
COMPOSITION

A Thesis

Presented to

The Faculty of Moss Landing Marine Laboratories

San José State University

In Partial Fulfillment

of the Requirements for the Degree

Master of Science

by

Diane E. Wyse

May 2014

The Designated Thesis Committee Approves the Thesis Titled

PLANKTON IN MONTEREY BAY:
OPTIMIZATION OF OPTICAL SENSOR DATA FROM AUTONOMOUS
UNDERWATER VEHICLES WITH APPLICATIONS IN PLANKTON COMMUNITY
COMPOSITION

by
Diane E. Wyse

APPROVED FOR MOSS LANDING MARINE LABORATORIES

SAN JOSÉ STATE UNIVERSITY

May 2014

Dr. Erika McPhee-Shaw	Moss Landing Marine Laboratories
Dr. Nicholas Welschmeyer	Moss Landing Marine Laboratories
Dr. James Bellingham	Monterey Bay Aquarium Research Institute

ABSTRACT

PLANKTON IN MONTEREY BAY:
OPTIMIZATION OF OPTICAL SENSOR DATA FROM AUTONOMOUS
UNDERWATER VEHICLES WITH APPLICATIONS IN PLANKTON COMMUNITY
COMPOSITION

by Diane E. Wyse

Autonomous underwater vehicles (AUVs) equipped with oceanographic sensors demonstrate the capability to describe plankton communities in the marine environment. The vehicles collect data from the surface through the mixed layer for a variety of oceanographic parameters. The Monterey Bay Aquarium Research Institute operates the *Dorado* upper-water-column AUV. The *Dorado* AUV collects data for 32 size-classes, from 1.25 to 250 μm, using a laser in-situ scattering and transmissometry (LISST-100X) instrument. The objective of this study was to analyze data from AUVs and laboratory work to inform sampling methods with applications in targeting specific classes of plankton, particularly harmful algal bloom species. The results of this study show that specific combinations of LISST-100X size class channels can be combined to reconstruct fluorescence data. This project included laboratory tests with monocultures of phytoplankton on both a backscattering sensor that detects chlorophyll at 695 nm and on the forward scattering LISST-100X sensor. The results show a linear relationship between backscattered chlorophyll concentration and cell density for four monocultures of phytoplankton. The forward scattering lab experiments show distinct organism signatures for three genera of phytoplankton tested as monocultures.

ACKNOWLEDGEMENTS

Contents

LIST OF TABLES

LIST OF FIGURES

1. Introduction

Primary productivity in the marine environment is driven predominantly by a combination of biological and physical processes. Spatial and temporal changes in ocean conditions contribute to variability in plankton community size and persistence. Plankton community composition is also driven by biogeochemical processes that include nutrient availability and uptake by marine organisms, as well as export by aggregation and vertical flux (Miller & Wheeler, 2012).

There are a variety of methods by which oceanographers can study primary productivity and biological activity in the upper ocean. Technology capable of *in situ* sampling of the ocean includes, among many other platforms, moorings with oceanographic and meteorological data acquisition instrumentation, shipboard underway systems, remote sensing via satellite imaging, stationary seawater intake systems, drifting platforms like the Wave Glider® and Slocum gliders, and autonomous underwater vehicles (AUVs) with propulsion systems. Each of these systems provides tremendous opportunities to study physical dynamics and biological processes in the marine environment, and data acquisition methods vary based upon research interest and user needs. A unique advantage for oceanographic sampling using propeller-driven AUVs is the ability to continuously sample a three-dimensional volume in a Lagrangian context. For example, the long-range AUVs operated by the Monterey Bay Aquarium Research Institute (MBARI) are capable of drifting with a parcel of water, or can propel up to one meter per second through the water column, depending on mission assignment (Bellingham et al., 2010).

In order to more fully understand and describe the oceanographic processes that affect primary productivity in the ocean, sampling strategies must be optimized for ocean conditions and plankton community dynamics. Remote sensing technologies provide data coverage over large spatial and temporal scales, but they are limited to sampling at the sea surface and data acquisition can be limited by cloud cover. AUVs are among the premier tools for optimized oceanographic sampling, due to their ability to sample adaptively, their extensive sensor suite, and coverage in three dimensions. In the case of the AUVs at MBARI, a vehicle's mission can be modified to follow specific oceanographic events and sample autonomously during the period of deployment (Zhang, McEwen, Ryan, & Bellingham, 2009). These features are critical tools for assessing and monitoring the physical processes influencing phytoplankton bloom dynamics and plankton community succession in the coastal marine environment.

This study seeks to address questions regarding plankton community composition through analysis of *in situ* data and laboratory calibration of optical sensors operated on AUVs in Monterey Bay. Results from this research can be applied to the optimization of sampling strategies in order to make a more definitive characterization of the biological composition of water masses encountered by AUVs in the coastal environment. In the first section of this study, data from two optical sensors on MBARI's *Dorado* upper-water-column AUV were analyzed to determine the extent to which the fluorescence signal from planktonic organisms can be reconstructed using particle size data. Data from the vehicle's fluorometer were analyzed and particle scattering data for six of the 32-logarithmically spaced channels between 1.25 and 250 μm from the LISST-100X

were combined to replicate, or reconstruct, the fluorescence signal with the least residual error. In the second section of this study, a laboratory sensor calibration was performed by testing monocultures of phytoplankton species in size classes below 250 μm in front of an optical backscatter and a forward scattering sensor. The data for chlorophyll-α concentration from optical backscatter at 695 nm were compared to laboratory cell density counts using instruments appropriate to the organism size. In the third section of this study, particle size distributions from forward scattering were analyzed to determine organism scattering signatures for monocultures of phytoplankton. The purpose of the laboratory experiments was to compare chlorophyll concentration to cell density and to investigate the extent to which distinct organism signature identification can be established using optical sensors for phytoplankton with various sizes and shapes. The organism signature information can be applied to improve analysis of *in situ* datasets from optical sensors deployed on AUVs in the coastal environment.

1.2 Background

1.2.1 Phytoplankton of Monterey Bay

Several studies of marine plankton have shown a shift in species composition associated with variability in nutrient dynamics. Corlett (1953) illustrates seasonal succession from diatom to dinoflagellate-dominated community structures. Barlow, Mantoura, Gough, and Fileman (1993) illustrated plankton community succession during a spring bloom in the North Atlantic, with diatoms dominating over the first 15 days, then prymnesiophytes and dinoflagellates increasing in abundance and dominating as the

diatom numbers diminish for days 16-45 of the bloom event. A study by Fawcett and Ward (2011) relating the total community diversity of samples in conditions mimicking Monterey Bay spring upwelling showed a community initially dominated by diatoms, with total community diversity increasing as diatom diversity decreased during the bloom event.

Marine diatoms typically range in size from 2 to 200 μm, well within the optical range of the LISST-100X sensor, and include two of the species of interest in this study, *Pseudo-nitzschia heimii* and *Pseudo-nitzschia australis* (Thomas, 1997).   The other two species of interest include a prasinophyte, *Micromonas sp.* and a haptophyte, *Heterosigma akashiwo*, both found in Monterey Bay (Bowers, et al., 2006, Worden & Not, 2008). Work performed by Rienecker et al. (2008) investigated various monoculture signatures using a LISST-100X, including *Pseudo-nitzschia australis*. That study found similar LISST-100X scattering signatures for *Pseudo-nitzschia* for both *in situ* and laboratory data. The study by Rienecker et al. also demonstrates two scattering peaks corresponding to the length and width axes of *Pseudo-nitzschia*. The two species of *Pseudo-nitzschia* tested in this study include *Pseudo-nitzschia heimii* and *Pseudo-nitzschia australis. P. heimii* is common in the autumn and winter on the west coast of the United States, while *P. australis* is more common in the autumn (Fryxell, Villac, & Shapiro*, 1997).

1.2.2 Physical Oceanography of Monterey Bay

Monterey Bay is characterized by various dynamics and variable conditions that drive primary productivity. In the springtime, and to a lesser extent in the fall, wind-driven coastal upwelling moves nutrient-rich deeper water towards the surface (Pennington & Chavez, 2000). There are three distinct oceanographic periods defined originally by Skogsberg (1936) and Skogsberg and Phelps (1946): an upwelling season in spring and early summer, an oceanic season in late summer and early fall, and a Davidson current season in the winter (Pennington & Chavez, 2000). During periods of upwelling, the oceanographic conditions are favorable for phytoplankton blooms (Pennington & Chavez, 2000). There is an upwelling center at the Año Nuevo promontory, and a shadow of that intensified surface signature can sometimes be seen in Monterey Bay (Woodson, et al., 2009). Fronts develop at the interface of two water bodies and are often characterized by steep gradients in temperature as well as chlorophyll (Ryan, McManus, Paduan, & Chavez, 2008). These fronts can develop thin phytoplankton layers, which have been studied recently through the development of an adaptive sampling algorithm on the *Dorado* AUV (Zhang et al., 2009). The ability of the vehicles to sample adaptively is central to the motivation for identifying organism signature IDs from *in situ* data sets in this study.

Another feature that affects nutrient transport in Monterey Bay and the adjacent Elkhorn Slough is the Monterey Submarine Canyon. The dynamics and composition of the upper water column can be affected by the dynamics and forcing in the benthic environment. Recent work by Carroll (2009), and Novak (2011) has described the effects

of internal waves on benthic turbulence and McPhee-Shaw amd Kunze (2002) have modeled those effects. Ongoing studies are investigating subsequent nutrient delivery associated with resuspension of sediments. A study by Ryan et al. (2010) found that intermediate nepheloid layers, characterized by high backscatter and low chlorophyll signal, and occurring below the mixed layer, transport invertebrate larvae episodically. Recent work by Ryan et al. (2013) investigated the effects on boundary intrusions and resuspension on HAB events. Cheriton et al. (2014) detected large particles (~ 34 μm) as a suspended particulate matter from the mudbelt of the continental shelf as far as 33m above the seafloor into the mid-water column. These studies highlight the importance of considering the dynamics, composition, and particle size distribution of both the upper water column and benthic environment when assessing plankton community structure.

1.2.3 Autonomous Underwater Vehicles in Oceanography

Developing, deploying, and successfully recovering AUVs is truly an interdisciplinary effort, even before any oceanographic or science instruments are added to the payload. Mission-critical decisions must be made prior to any deployment, so an investigation into the data obtained is critical to successful vehicle use in the future. A goal of AUV research is to optimize the available power for propulsion and instrument operation, as a system for recharging an AUV during a mission is not currently viable. For this reason, scientific inquiry into *in situ* data is valuable for both better understanding ocean conditions and making decisions about the continuous operation of a sensor with regards to a vehicle's energy budget.

The *Dorado* AUV has a deployment time of 12-18 hours, though it can be

deployed and recovered multiple times from a ship during a bloom event. On its primary

lithium batteries, the LRAUV has the capability to deploy for nearly a month (26 days)

uninterrupted, which could provide for more thorough, continuous coverage of a bloom

event than a shorter-range vehicle. Developing sampling techniques from analysis of the

Dorado vehicle data that can be applied to the LRAUVs is useful in extending the time

for uninterrupted *in situ* sampling. The *Tethys* class LRAUVs, designed by engineers and

researchers at MBARI, are capable of performing Lagrangian sampling at depths up to

300m. These vehicles, equipped with a suite of optical oceanographic sensors, are

valuable tools for better characterizing ocean water composition and physical dynamics.

In this project the terms "vehicle deployment" and "mission" are both used to describe

the period during which an AUV is sampling continuously in the marine environment.

The AUVs operated by MBARI perform "yo-yo" sampling by moving up and down the

water column as it moves along the path of the mission, a similar concept to a person

walking and spinning a yo-yo, but on a larger spatial and temporal timescale. The

vehicle changes depth in the water column by changing its ballast, in the case of the

LRAUV the heavy batter pack sits on an elevator attached to the motor that changes the

vehicle's pitch. The LRAUV and *Dorado* class AUVs are depth-rated to 300 m.

The Controlled Agile and Novel Ocean Network (CANON) initiative is an

interdisciplinary MBARI activity aimed at improving understanding of biological and

physical ocean dynamics by targeted sampling with multiple platforms (Das et al., 2012).

The AUVs and LRAUVs are actively deployed for the CANON missions to collect

continuous data in three dimensions. Data analyzed in the first part of the project were obtained from two deployments of the *Dorado* AUV during the May 2012 CANON project.

1.2.4 Optical Sensing in Oceanography

Optical instruments are used in oceanography to describe many features of water composition from sediment concentration and transport near the benthic environment, to particle size and volume concentration for community composition in the upper water column. A major benefit of optical sensors is the ability to describe water composition with large spatial coverage. Depending on the design and nature of the instrument, optical sensors can detect particle sizes, water turbidity, and volume scattering distributions of particles in seawater. Other advantages of optical instruments in oceanographic studies include providing continuous data output with relatively low energy demand, compact and portable size, and particle detection limits at sizes below those of acoustic devices. According to Lynch, Irish, Sherwood, and Agrawal (1994), the lower detection limits of acoustical devices is around 25 μm diameter particles. One of the optical sensors used in this research, the LISST-100X, can detect classes of plankton in the picoplankton realm to microplankton, 1.25 to 250 μm, a size detection range encompassing two orders of magnitude.

Fluorescence is characterized by the absorption of light at one wavelength and re-emission at a longer wavelength (Suggett, Moore, & Geider, 2011). Fluorescence is often measured in the marine environment to detect chlorophyll-α and is useful for estimates of primary productivity (Suggett, et al., 2011). Research performed in Genty,

Briantais, and Baker (1989) quantified the linear relationship between measurements of fluorescence and CO_2 fixation, establishing the relationship between fluorescence and productivity.

The optical instruments of interest in this study include a HydroScat-2 Backscattering Sensor and fluorometer, the Environmental Characteristics Optics (ECO) Puck, and the LISST-100X. The Hydroscat sensor used by MBARI on the *Dorado* AUV for the 2012 CANON deployments records backscatter at two wavelengths, 420 and 700 nm, and fluorescence at 420 nm. Designed by WET Labs as a compact and portable sensor, The ECO puck emits light to excite particles, and the model used in this study measures optical backscatter at 470 nm, 650 nm, and 695 nm. The scattering measured at 695 nm includes excitation of chlorophyll-α at 470 nm and emission at 695 nm, and is used to calculate chlorophyll concentration in μg/L using Equation 1. All LISST-100X data in this experiment come from a Type B instrument, which measures particle size distributions and volume concentrations between 1.25 and 250 μm. Each of the instruments used in this study are commonly deployed with the upper-water-column *Dorado* AUV, while the ECO puck fits with other oceanographic sensors on the smaller *Tethys* LRAUVs.

The HydroScat fluorometer used in this study emits light at the excitation wavelength for chlorophyll-α and detects the longer wavelength that is emitted. Specifically, the instrument has two light-emitting diode (LED) lights, one for blue and one for red light, and corresponding detectors approximately 2 cm from the respective source lights (HydroScat-2 User Manual, 2011). The two source-detector arrays are

arranged perpendicular to each other, so that the beams cross at a 90° angle (Figure 1).

The backscatter detection wavelengths for the instrument used in section 1 are 420 nm

and 700 nm. Due to the crossing beam design of the instrument, the 700 nm detector also

detects fluorescence from the 420 nm light scattered onto the 700 nm detector (Figure 1,

HydroScat-2 User Manual, 2011). The HydroScat fluorometer is not calibrated to an

absolute fluorescence standard, so the fluorescence data in section 1 of this research are

presented as relative fluorescence units (RFU).
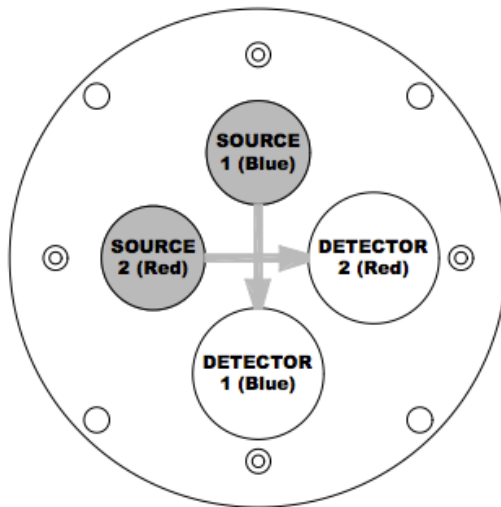
Figure 1. HydroScat-2 optical sensor. The cartoon illustrates the cross-beam design that
permits detection of fluorescence on the 700 nm (blue) wavelength detector. Reprinted with
permission from Hobi Labs (HydroScat-2 User Manual, 2011).

According to characteristic length approximations established by Sieburth et al.

(1978), the plankton sizes that can be detected by the LISST-100X include picoplankton

(0.2 – 2 μm), nanoplankton (2 – 20 μm), microplankton (20 – 200 μm), and potentially

some smaller classes of mesoplankton (200 – 20000 μm). Designed by Sequoia

Scientific, Inc., the LISST-100X uses laser diffraction to measure the volume concentration and scattering distribution of particles on a ring detector plate with 32 logarithmically-spaced rings. Raw ring count data for the 32 ring detectors must be processed with an inversion algorithm, provided by Sequoia and performed in Matlab, that converts count data to volume concentration distribution. The processed data can be plotted with mean particle diameter to determine particle scattering distribution. The inversion algorithm provided uses the principle of Mie scattering to determine particle size using angle of diffraction. Sequoia provides mean particle diameter data for each of the 32 channels for data processed as "spherical" or "randomly shaped" particles. In the first section of this study, the inversion from raw ring intensity counts to particle scattering distribution was performed for all laboratory samples assuming spherical particles so that data can be analyzed using the inversion algorithm provided by Sequoia. The LISST-100X laser is a 670 nm solid-state diode with a pathlength of 5 cm. The scattering angles are 0.08 to 15º in water.

The particle size distributions measured from LISST-100X scattering correspond to the multiple angles of scatter associated with the biological organisms and other particles that pass through the path of the laser. The instrument has many applications in sediment transport studies; research performed in Gartner, Cheng, Wang, and Richter (2001) suggests that the instrument can be used to describe sediment transport in San Francisco Bay. Agrawal and Pottsmith (2000) describe the capability of the instrument to measure settling velocity.

One limitation to plankton classification using a LISST-100X is the size class data do not automatically distinguish length from other plankton morphometrics; the sensor readout simply gives raw intensity counts for the 32 rings, which are processed through an inversion algorithm to give particle size distributions with volume concentrations. Laboratory tests performed by Rienecker et al. (2008) indicate two peaks in the particle scattering data using monocultures of the genus *Pseudo-nitzschia*, one possibly associated with cell length and the other with cell width, suggesting that taxon-specific organism identification is possible using the LISST-100X. An understanding of cell morphology is necessary for proper interpretation of LISST-100X data in a biological context. In the laboratory experiments of this thesis, microscope counts and cell sizes were determined to understand cell morphology and compare monoculture densities to optical concentration values and scattering signatures. The value of this work is the ability to relate multiple sensor data to describe monocultures with applications in interpreting *in situ* data during events dominated by a certain genus of phytoplankton.

1.2.5 Optical Theory and Mie Scattering

The LISST-100X uses principles of Mie scattering theory to quantify particle size and volume concentration. The basics of Mie scattering indicate that the angle of diffraction of a spherical particle is inversely related to the particle size (Stratton, 1941). For example, a larger particle will yield a smaller angle of diffraction, while a smaller particle will diffract at a larger angle of diffraction.

1.4 Objectives and Scope of Project

The objective of this research was to enhance understanding and improve analysis of optical sensor data for characterization of phytoplankton community composition in Monterey Bay. Analysis of measurements from bench-top laboratory instruments and vehicle optical sensors were performed to determine organism signature identification and to attempt to characterize community composition from *in situ* optical sensor data collected during CANON missions. An application of this study is to improve sampling techniques to autonomously track phytoplankton bloom events and more thoroughly describe plankton community structure using optical sensors. The following research questions were addressed in this project:

1) Can combinations of LISST-100X size class data be combined to reconstruct fluorometer data from the *Dorado* AUV? If so, how effectively does the reconstructed signal match the fluorescence signal?

2) What is the relationship between laboratory counts of cell density for both the ECO puck chlorophyll concentration data and the LISST-100X particle scattering distributions for monocultures of phytoplankton?

3) Do optical sensors give clear organism signatures when algal monocultures are interrogated?

4) How definitively do the organism signatures determined from laboratory tests describe a phytoplankton population or bloom event from *in situ* data?

2. Methods

2.1 Optical Sensor Relationships LISST-100X and HydroScat Fluorometer

In summer 2012, in conjunction with the MBARI summer internship program, I analyzed data from two optical scattering sensors mounted on the *Dorado* AUV during a CANON mission. My research assessed the relationship of particle scattering to optical fluorescence data in the context of the ability of the LISST-100X particle size data to reconstruct HydroScat fluorescence data. The data analyzed here are from two deployments during the May 2012 CANON mission in Monterey Bay.

The objective for this study was to determine whether a small grouping of LISST-100X particle size channels could be combined to reconstruct the fluorescence data from the HydroScat fluorometer. To further investigate size channel reconstruction of fluorescence, and to determine whether different size channels dominated different fluorescence intensities, I split the data sets into three subsets by time during periods of low and high fluorescence. The first channel in the combination analysis represents 90% of the reconstruction of the fluorescence signal, with the remaining channels contributing to the reconstruction to a lesser extent.

I performed all analyses of *Dorado* optical sensor data in Matlab. The data were preprocessed and provided by Dorota Kolber at MBARI. The time variable for mission data comes from the time recorded on the HydroScat fluorometer. To process the data for analysis, negative values for the fluorescence signal were removed and listed as "NaN" (not a number) in the Matlab script. The remaining signal data were despiked using an algorithm, "findspike," programmed by Dr. Bellingham. Time and LISST-100X data were then interpolated using the interpl.m function to match variable length for surrogate reconstruction.

2.2 Laboratory Sensor Tests: LISST-100X and ECO Puck

In summer and fall of 2013, I performed laboratory sensor calibration on the ECO puck backscatter sensor and LISST-100X particle size distribution sensor. The tests were conducted to determine organism signatures and chlorophyll concentration from optical backscatter for fluorescing plankton between the sizes of 1.25 and 250 μm. To perform the experiments, I cultivated monocultures of *Micromonas sp.*, *Heterosigma akashiwo*, *Pseudo-nitzschia heimii,* and *Pseudo-nitzschia australis* in the laboratory at MBARI. Culture details, including cell size, density, and shape are listed in Table 1.

The ECO puck collects data by shining lights at three wavelengths, 470 nm, 650 nm, and 695 nm, with three detectors that receive scattering from particles in the water. Data collection for the ECO puck was performed using the software disk provided by WET Labs.

Data were collected for the LISST-100X using the LISST standard operating (SOP) procedure software downloaded onto a Windows-compatible desktop computer in the LRAUV lab.

2.2.1 Culture Strain Information

The *Micromonas sp.* culture was isolated in axenic conditions from Bigelow Laboratory strain 2.9RCC299 (Table 1). The culture was grown in F/2 culture media, detailed in 5.2b, and kept in a 21ºC incubator on a 14:10 light cycle. The *Heterosigma akashiwo* culture was obtained from the North East Pacific Culture Lab (NEPCC), Vancouver, Canada and provided by the Scholin Lab at MBARI. The culture was grown in F/2 culture media and kept in a 21ºC incubator on a 14:10 light cycle. Chlorophyll concentration and cell density data from flow cytometry counts for *Ostreococcus sp.* are included in the results of section 3.2 but not included in Table 1 as size approximations for *Ostreococcus sp.* were not obtained in the lab, and Table 1 details the four monocultures tested on both the ECO puck and LISST-100X. *Ostreococcus sp.* is a globally-distributed prasinophyte green alga that is less than 2 μm in size (Countway & Caron, 2006). The *Ostreococcus sp.* culture was grown in F/2 culture media and kept in a 21ºC incubator on a 14:10 light cycle. *Micromonas sp.*, *Ostreococcus sp.*, and *H. akashiwo* were grown and analyzed with support from the Worden/microbial ecology lab and the LRAUV lab during summer 2013.

The *Pseudo-nitzschia heimii*, lab sample "*P. heimii* 6," was isolated by Holly Bowers from a water sample collected on the San Pedro shelf, March 15th 2013, at 18 meters.

The culture was grown in F/2 culture media, detailed in 5.2c, and kept in a 15ºC

incubator on a 14:10 light cycle. The *Pseudo-nitzschia australis*, lab sample "*P. australis*

123" was isolated by Holly Bowers from Dorado gulper bottle #5, fired at 15.4 m depth

on the San Pedro shelf, March 16th 2013. The culture was grown in F/2 culture media,

detailed in 5.2c, and kept in a 15ºC incubator on a 14:10 light cycle. The *Pseudo-*

nitzschia cultures were generously provided by Dr. Bowers and kept in the Scholin lab

during experiments in fall 2013.

2.2.2 Preparation of F/2 Culture Media

Methods for cultivation of *Micromonas* and *Heterosigma* followed NCMA protocol:

1) Load GFF and 0.2μm filter
2) Mix 900 mL CANON II (CAS 138 (40CH1) water with 100 mL Milli-Q
3) Filter water, with bag over top to avoid getting dust in the sample, using gas pump ~0.4 bar
4) Salt addition: F/2 CCMP kit (21 Dec 2011)
    a. Phosphate, Trace Metal, Nitrate, Silicate, 500 μL vitamins from SUCX:14 (Sebastian Sudek's mix)
5) Add acid. 600 μL 3.7% HCl
6) Split culture media between two bottles to autoclave. Autoclave on liquids cycle (4) for 55 min. Allow media to cool completely before adding to organism cultures. Store on clean lab shelf in the dark.

Methods for cultivation of *P. heimii* and *P. australis* followed procedure developed in

Guillard and Ryther (1962), and Guillard (1975).

2.3 ECO Puck Laboratory Sampling Apparatus

The ECO puck sampling chamber was developed in-house at MBARI by

Research Specialist Denis Klimov in July 2013. The chamber was made of 0.5" thick

black expanded polyvinyl chloride (PVC) panels glued together on top of a 6x9" black expanded PVC base. The apparatus was developed water-tight and remained as such over the course of the experiment from August 2013 through January 2014. The experiments for the ECO Puck were conducted using 600 mL of filtered seawater and increasing concentrations of monoculture sample, such that the face of the puck would be as far as possible from the bottom of the chamber while minimizing the volume of water and monoculture necessary to test. A box-shaped lid of optically-black foil was placed over the top opening of the sampling chamber in order to minimize the effects of background light on the experiment. The face of the ECO puck, including excitation lights and detectors, stood 2.5 inches above the bottom of the sampling chamber when propped on 0.5 inch expanded PVC on top of the edges of the sampling apparatus.

To investigate concerns regarding optical clarity, several water sources were tested on the instrument using the sampling apparatus. Filtered seawater was used for the tests performed in this experiment. The *Micromonas* and *Heterosigma* tests were conducted in filtered, autoclaved artificial seawater, whereas the *Pseudo-nitzschia* samples were tested in filtered Monterey Wharf water. The sampling apparatus was tested with several different water sources, including Milli-Q water, filtered seawater, filtered test tank water, and filtered artificial seawater.
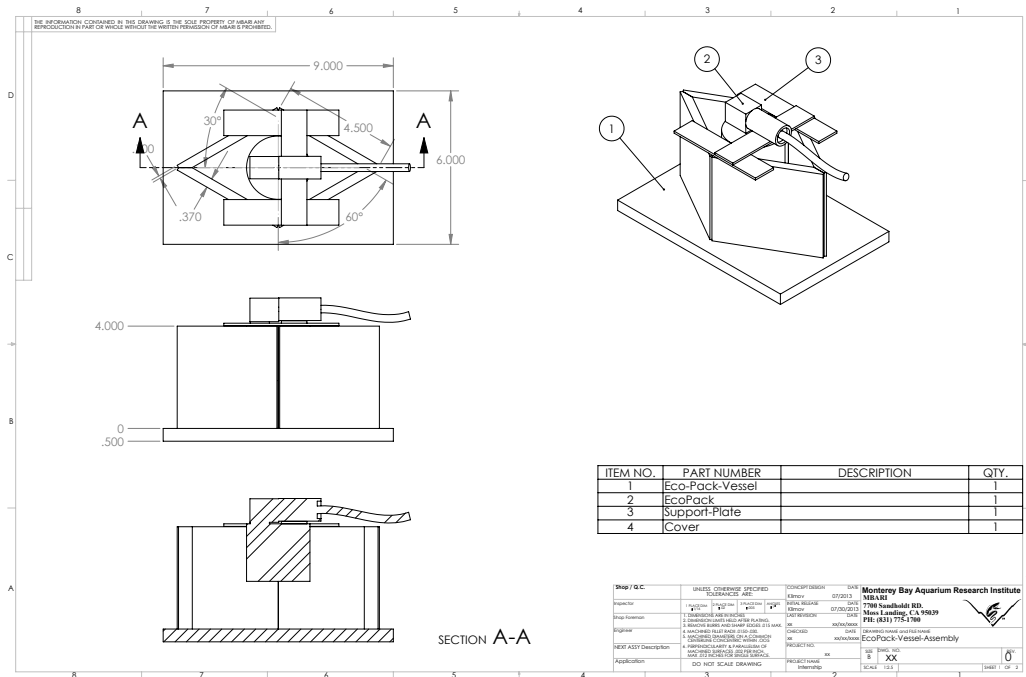
Figure 2a. ECO Puck sampling chamber design by MBARI Electrical Engineer Denis Klimov/MBARI 2013. Reprinted with permission from D. Klimov.
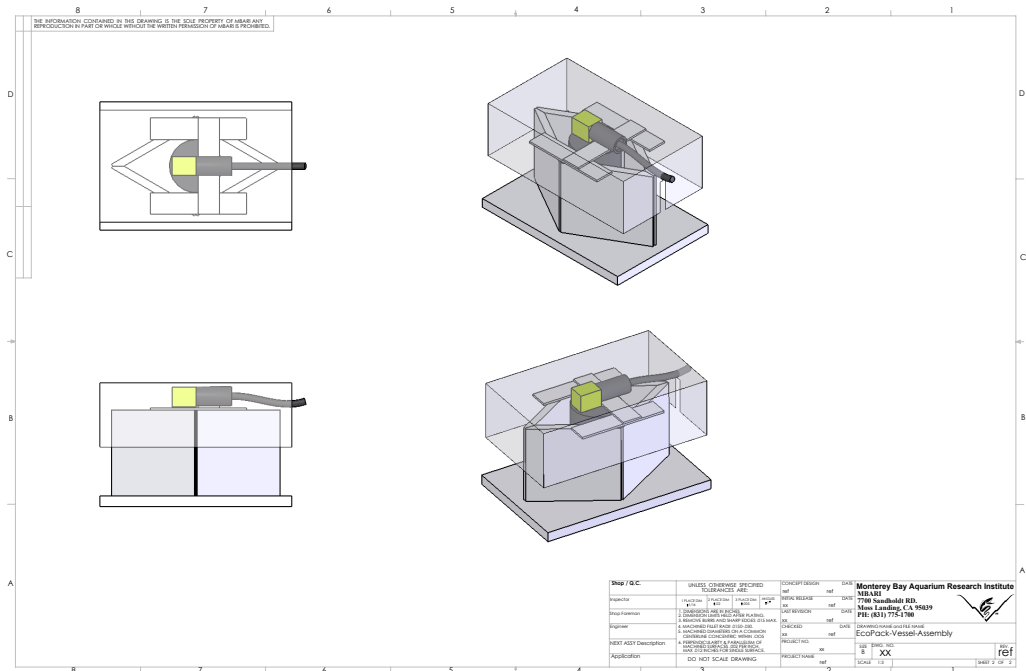
Figure 2b. ECO Puck sampling chamber design with foil cover by MBARI Electrical Engineer Denis Klimov/MBARI 2013. Reprinted with permission from D. Klimov.
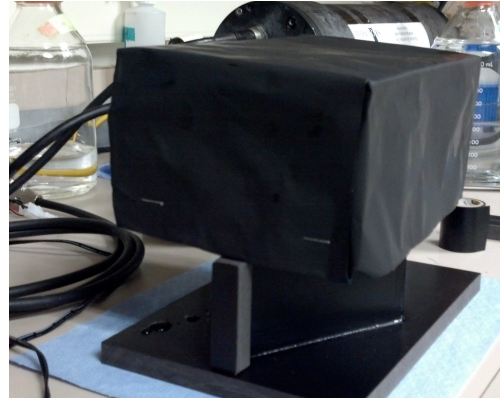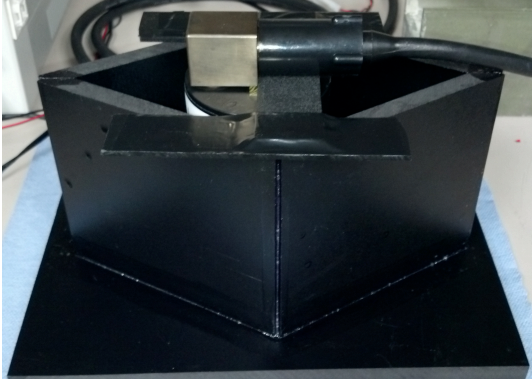
Figure 3. ECO Puck sampling apparatus in the Long-Range AUV Lab, developed by D. Klimov (2013).

2.4 LISST-100X Sampling Cell

The sampling chamber used for the LISST-100X lab tests was the black ~100 mL capacity cell provided with the instrument for laboratory calibration. A 4" tube with a plug was attached the outflow of the chamber to regulate volume during the experiment. Before each experiment the LISST-100X optical window was cleaned with isopropyl alcohol and the chamber was fully rinsed with Milli-Q water. A piece of optically-black foil was placed over the top opening of the sampling cell in order to minimize the effects of background light on the experiment.
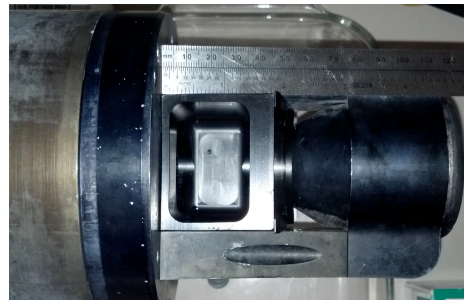
Figure 4. Aerial view of LISST-100X sampling cell. A black foil cover was placed over the cell to minimize interference by ambient light.

2.5 Laboratory Experiments

2.5.1 Optical Backscatter Sampling Procedure, ECO Puck

Several methods were tested to sample with the ECO puck in the lab. Preliminary tests were performed in a 1-L graduated cylinder beaker, with optically-black foil lining the sides. This design was intended to maximize the distance from the detector face to the bottom of the container and minimize reflection from the bottom of the sampling chamber, while minimizing the amount of seawater and culture sample necessary to perform the tests. The foil had to be changed for each culture tested, to minimize opportunity for contamination from a previous culture tests. A more permanent option was made available when the diamond-shaped sampling apparatus was designed.

Each monoculture test performed in the PVC sampling apparatus followed the same pattern. I took a dark counts measurement by covering the three detectors with black electrical tape and leaving the lights exposed. My method for determining dark counts follows the findings of Cetinić et al. (2009) as the most accurate method for determining dark count values for the ECO puck. I averaged and compared the dark count values for the three wavelengths to factory settings. Next, I took a background measurement was taken using 600 mL of 0.22 μm-filtered Milli-Q water. In each test, I collected 25 samples at 1.01Hz using the WET Labs software package on a desktop computer. The data for optical backscatter were detected at 470 nm, 650 nm, 695 nm, and thermistor values collected, copied, and saved to Excel for data analysis. I emptied the sampling chamber of the Milli-Q water to prepare for the filtered seawater and monoculture tests.

The next step of sampling involves measuring the background values for filtered artificial seawater. I prepared the artificial seawater in the Worden lab using 1 L of Milli-Q water and 40 g of Sigma-Aldrich sea salts. The artificial seawater was autoclaved to minimize contamination of the monoculture in the experiments, then cooled to room temperature. I filtered the artificial seawater the day of the lab tests to prevent culture contamination by bacteria or other potential contaminants. To determine the filtered artificial seawater (fASW) background on the ECO puck I added 600 mL of filtered artificial seawater to the sample chamber. In each consecutive experiment for the ECO puck the data were copied from the software output and saved to Excel for analysis.

To test the monocultures, an initial volume was pipetted into the puck chamber and the first 25 scattering samples were collected at 1.01 Hz and saved to Excel for analysis. The initial volume varied between the different cultures tested, for example the first test for *Micromonas sp.* (Figure 17) had 0.3 mL of monoculture into 600 mL of fASW. The initial volume of *P. australis* 1 on (Figure 25) was 3 mL into 600 mL. The different initial volumes among the monoculture tests was determined based upon the total culture available. Before running each experiment a decision was made regarding the initial volume of culture to add to the sampling chamber in order to test at least four different culture concentrations per experiment, with enough culture left to perform two concentration experiments on the LISST-100X. Next, a higher volume of the same culture was pipetted into the sample chamber, and continued the sampling procedure until the maximum desired concentration was tested. After the highest culture concentration test on the ECO puck, a subsample of 100 mL form the puck sampling chamber was

transferred into the LISST-100X sampling chamber using a graduated cylinder. This step

was performed to have a point at which both instruments could interrogate the same

concentration in each monoculture test. For the *Pseudo-nitzschia* cultures tested in the

laboratory all samples were measured and transferred by pouring into a graduated

cylinder, instead of pipetting, as pipetting would break up the healthy cell chains.

2.5.2 Forward Scattering Sampling Procedure, LISST-100X

To test the particle scattering distributions and volume concentrations of

monocultures of phytoplankton, I set up MBARI's AUV lab's LISST-100X in the

LRAUV lab. I set the instrument on a fiberglass stand and placed a black sampling

chamber around the optical sensing end to test increasing concentrations of each

monoculture. The volume of the sampling chamber is approximately 100 mL, and is

equipped with a small drainage hole, which Denis Klimov assisted in adding a short tube

and plug for sampling. I connected the instrument to a desktop computer in the LRAUV

lab and queried the instrument using the LISST standard operating procedure (SOP)

software. I also accessed the SOP software to collect background scattering, or "zero

scattering" (zscat) data before each test using 0.22 um filtered Milli-Q water. The

purpose of collecting the background or zscat file prior to each experiment is to

determine whether the optical face is clean and the laser is properly aligned and has high

enough power to sample effectively. If the zscat test returns high concentrations at any of

the rings it could be indicative of a dirty optical window, which can be cleaned with

ethanol. If the laser power is below 25% of factory settings, it may be indicative of misalignment, in which case the instrument must be returned to Sequoia for realignment.

To obtain background scattering with the LISST-100X, I rinsed the sampling chamber with Milli-Q water to remove any dust around the optical sensor. I poured 100 mL of Milli-Q into the chamber and covered it with optically black foil to prevent interference from ambient light.   I then had the LISST SOP collect background, which yields an averaged output from 20 consecutive samples. The values obtained for the 32 rings plus the laser output are compared to the supplied factory zscat, which must be loaded before collecting background. In these experiments, I loaded the factory_zscat_1395.asc file for background scattering comparison. The SOP requires a choice between sampling as spherical or randomly shaped particles. I chose to process the data as spherical particles for all tests as the data processing method provided by Seqouia utilizes Mie scattering for inversion from ring intensity counts to particle scattering distribution.

Table 1. Monocultures of phytoplankton cultivated in the laboratory for optical sensor tests.
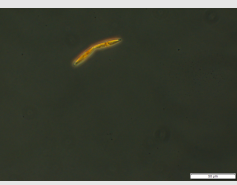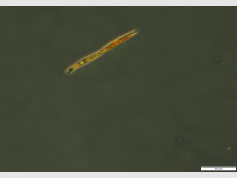
Cell Image	Strain	Monoculture	Cell Length (µm)	Cell Width (µm)	Shape
	2.9RCC299	*Micromonas sp.*	< 2	< 2	spherical
	NEPCC	*Heterosigma akashiwo*	18-34	18-34	oblong
	P. heimii 6 18 m depth	*Pseudo-nitzschia heimii*	30-100	3-5	pennate
	P. australis 123 15.4 m depth	*Pseudo-nitzschia australis*	50-100	3-8	pennate

Photo of *Micromonas sp.* by Deerinck, Terada, Obiyashi, Ellisman, &Worden (2009) http://www.mbari.org/news/news_releases/2009/micromonas/micromonas.html. Photo of *Heterosigma akashiwo*: Guiry, M.D. & WoRMS/Creative Commons (2013). Photos of *P. heimii* and *P. australis* by Diane Wyse/MBARI 2014

Table 2. Data relationships between instruments tested in this study.

| Instrument | Optical Backscatter | | Forward Scattering | | | |
	420 nm	700 nm	Particle Scattering Distribution	Chl-α	Organism Count	Cell Size
Accuri flow cytometer			✓	✓	✓	✓
Microscopy					✓	✓
HydroScat-2	✓	✓				
ECO Puck	✓ (470 nm)	✓ (650 nm)		✓		
LISST-100X			✓			

Each instrument is listed with type of data output.

For comparison of processed particle size data for LISST-100X against lab cell density counts, Accuri flow cytometric analysis was performed for of monocultures of *Micromonas sp.* and *Ostreococcus sp.* with assistance from Sebastian Sudek and Jian Guo in MBARI's Microbial Ecology (Worden) Lab. Microscope cell counts were performed for for 1 mL samples of Lugols-preserved *Heterosigma akashiwo*, *P. heimii,* and *P. australis* on a Zeiss microscope using a Sedgewick rafter.

An initial investigation was performed to determine whether raw ting intensity counts from LISST-100X data for each monoculture gave a clear organism signature. In those experiments, ring intensity was plotted against channel number (1-32) for *Micromonas* and *Heterosigma* samples, and broad peaks were identified around different groups of channels for each organism test, and increasing ring intensities with increasing concentrations. Those results were encouraging for finding an organism signature with LISST-100X particle scattering distribution (PSD) data. The analysis then proceeded to determine organism signatures from PSD for *Micromonas*, *Heterosigma*, *P. heimii*, and *P. australis* monocultures.

3. Results

The data presented in this chapter are grouped into three parts in conjunction with the three major datasets collected and analyzed. In the first section, data are presented for fluorescence signal reconstruction by particle size channels, performed during the 2012 MBARI summer internship program. The second section of results quantify the relationship between chlorophyll concentration from optical backscatter using the ECO puck and cell density data from laboratory counts for monocultures of phytoplankton. The third section characterizes organism signatures for four monocultures using particle scattering distribution data from a forward scattering sensor, the LISST-100X.

The first set of results comes from my summer 2012 MBARI internship project in which we successfully reconstructed *in situ* HydroScat fluorometer data from LISST-100X particle size data channels. The signal reconstruction algorithm developed by Dr. Bellingham minimizes the residual error between the two datasets by combining size channels that most closely match the fluorescence data over the course of the *Dorado* AUV's mission. The optical fluorescence data serve as a proxy for chlorophyll concentration; thus, the ability to recreate the fluorescence values using particle scattering data has implications for adaptive *in situ* sensing. If LISST-100X data are processed during a mission and a fluorescence value and scattering signature of interest are combined then the vehicle can be programmed to track those conditions during a mission.

The successful fluorescence signal reconstruction with particle scattering data was my primary motivation for pursuing laboratory work with monocultures of phytoplankton. In the second and third sections of my thesis results, I seek to determine organism signature

identification for four species of interest commonly found in coastal waters, including Monterey Bay, using a backscatter and forward scattering sensor. The first species is a picoeukaryote (diameter <2 um) with a global distribution, *Micromonas sp*., chosen to determine organism signature for a spherical shaped cells at the lower size limits for particle scattering distribution (PSD) on the LISST-100X (Worden & Not, 2008). The second species, *Heterosigma akashiwo*, is an ichthyotoxic alga chosen to determine organism signature for a pear-shaped fluorescing organism well within the size limits of the LISST-100X (Frederickson, et al., 2011). The third and fourth species, *Pseudo-nitzschia heimii* and *Pseudo-nitzschia australis*, were chosen as because of their implications as harmful algal bloom species (Fryxell, et al., 1997). These organisms also represent a different morphology than the first two species tested, and represent chain-forming pennate organisms.

3.1 Surrogate Reconstruction of Fluorescence Data

In summer 2012, I analyzed data from the May 2012 Controlled, Agile, and Novel Observing Network (CANON) initiative experiment to determine whether the *in-situ* data from the LISST-100X could reproduce the *in situ* fluorescence signal. The fluorescence signal was an optical measurement for excitation at 420 nm recorded by a HydroScat fluorometer during vehicle deployment. The particle scattering distribution data was measured by a LISST-100X instrument Type B, with logarithmically-spaced ring detectors that determine volume concentration distribution between 1.25 and 250 μm. Both of the instruments in this study were mounted on the *Dorado* AUV operated by MBARI and data were provided by Dorota Kolber.

This research determined that combinations of LISST-100X channels can reproduce the fluorescence signal with minimal residual error (Table 3). The different fluorescence intensities are characterized by different combinations of channels, suggesting that on a community scale, certain particle size distributions dominate with certain fluorescence levels. The first channel listed in Table 3 accounts for 90% of the reconstruction, and the other 5 channels contribute to the remaining 10% of the surrogate reconstruction of the fluorometer data.

Table 3. Summary of particle scattering distribution channels data.

Data File	Subset	Dominant LISST Channels			R^2, p value: fluorescence vs surrogate	Residual Error (iterative)	
Dorado 150 (May 2012 CANON)	Full Dataset: May 29, 2012 22:00:20 to May 30, 2012 11:58:07	20 3 31 8 5 13			0.8132, $p < 0.001$	0.0760 0.0737 0.0732 0.0694 0.0681 0.0663	
	First Subset: May 29, 2012 22:00:20 to May 29, 2012 23:48:20	20 2 12 32 5 17			0.78622, $p < 0.001$	0.0556 0.0551 0.0531 0.0528 0.0527 0.0511	
	Second Subset: May 29, 2012 23:48:20 to May 30, 2012 04:54:54	7 30 31 29 32 3			0.04633, $p < 0.001$	0.1040 0.1047 0.1063 0.1039 0.1045 0.1050	
	Third Subset: May 30, 2012 04:54:54 to May 30, 2012 11:58:07	20 4 31 8 6 14			0.81211, $p < 0.001$	0.0785 0.0744 0.0735 0.0687 0.0672 0.0654	
Dorado 151 (May 2012 CANON)	Full Dataset: May 30, 2012 20:53:02 to May 31, 2012 15:46:30	20 1 31 5 4 6			0.84568, $p < 0.001$	0.0967 0.0709 0.0654 0.0664 0.0680 0.0701	
	First Subset: May 30, 2012 20:53:03 to May 31, 2012 03:32:06	14 2 32 5 4 6			0.83038, $p < 0.001$	0.1413 0.0884 0.0850 0.0861 0.0871 0.0880	
	Second Subset: May 31, 2012 03:32:06 to May 31, 2012 07:00:54	7 1 2 3 12 11			0.00088, $p = 0.08$	0.0695 0.0723 0.0804 0.1043 0.1862 0.5127	
	Third subset: May 31, 2012 07:00:54 to May 31, 2012 15:46:30	20 4 3 32 6 11			0.8567, $p < 0.001$	0.0495 0.0533 0.0481 0.0475 0.0458 0.0428	

When combined, PSD channels match the fluorescence signal with the least residual error. Coefficient of determination, or R^2, values for scatterplots of fluorescence signal vs. surrogate reconstruction are provided for Figs. 7b, 8b, 9b, 10b, 13b, 14b, 15b, & 16b. The two data files represent two *Dorado* AUV deployments. Dorado 150 sampled for approximately 14 hours from May 29-30, 2012. Dorado 151 sampled for approximately 18 hours from May 30-31, 2012. Each Dorado mission is split into subsets based upon periods of continuous high and low fluorescence, as indicated in Figs. 8a, 9a, 10a, 14a, 15a, 16a. All times are in PDT.

To analyze fluorescence and PSD reconstruction data for the two CANON deployments in May 2012, I used Matlab and a script provided by Dr. Bellingham to determine PSD surrogates. The surrogate reconstruction script selects a combination of the six PSD channels that fit to the fluorescence signal with the least residual error. In each experiment the program determined the channels which best reconstruct the full dataset. After processing the full dataset for each mission, I manually chose time periods of large, consistent changes in fluorescence signal, when the fluorescence signal changed from high to low values, or from low to high values for periods longer than the yo-yo sampling variability. The periods of high fluorescence range from approximately 5E-4 to 6E-3 fluorescence units. The periods of low fluorescence include persistent values below 5E-4 fluorescence units (Figs. 7a and 13a). I used a switch loop to choose subsets of the data, based upon time periods during which the fluorescence remained consistently high or low. The signal and surrogate reconstruction variable sizes were both set to match the time period length of each subset.

To determine the relationship between the fluorescence signal and PSD reconstruction I scattered fluorescence data against the PSD reconstruction and fit a line to the data. Through Mathworks I found a coefficient of determination script provided by J.R. Wells, RSQUARE, that produces scatter plots with a linear calculation of the fluorescence vs. PSD relationship. The RSQUARE function calculates positive, logical R^2 values for all eight plots of fluorescence signal vs. PSD reconstruction (Table 3, Figs. 7b, 8b, 9b, 10b, 13b, 14b, 15b, and 16b). The RSQUARE function determines R^2 using

31

real data for y (in this case, fluorescence signal) and model data for f (surrogate

reconstruction data), with a constant term in the model (c=1).

```
function [r2 rmse]


if c; r2 = max(0,1 - sum((y(:)-f(:)).^2)/sum((y(:)-
mean(y(:))).^2));
else r2 = 1 - sum((y(:)-f(:)).^2)/sum((y(:)).^2);

x = surrogate;
y = signal;
p = polyfit(x,y,1);
f = polyval(p,x);
[r2 rmse] = rsquare(y,f);
```

The figures below are presented using the RSQUARE function calculation to

report logical R^2 values for subset 2 in each *Dorado* dataset. The p values reported for

each dataset were determined using the regression diagnostics function 'regstats' in

Matlab for a linear model. A p value below 0.05 indicates that the relationship between

the reconstruction model fluorescence data is unlikely to have occurred by chance. In all

but two of the datasets tested, $p < 0.001$ (Table 3). The only $p > 0.05$ was determined for

the second subset of *Dorado* 151, where $p = 0.08$ (Table 3). Figs. 5-16b explain the

analysis steps taken to reproduce the fluorescence signal using particle scattering

distribution data. First, I plotted the Hydroscat fluorescence data as I received it (Figs. 5

and 11). To process the data, I removed the NaN's ("not a number," no data at those

points), removed all negative values for fluorescence, and removed spikes (Figs. 6 and

12) from the raw fluorescence data. Figs. 6 and 12 are included to show the data

removed using the findspike function provided by Dr. Bellingham with a threshold value

of 20. The function removes most of the outlier spikes, but also removes some of the

data points within the reasonable fluorescence values, based upon the threshold value

selected by the user. I chose a threshold value of 20 for both *Dorado* fluorescence

datasets as it maximized the spikes removed without taking out too many good data

points. The spike values in red (Figs. 6 and 12) are calculated where the height of the

data point is greater than the median height multiplied by the threshold, and where the

absolute value of the difference between adjacent data points is less than the median

height multiplied by threshold. Spike2, in blue, refers to all data where height is greater

than the median height multiplied by threshold value. In the figures showing PSD

reconstruction with fluorescence data (Figs. 7-11a, 13-16a) the residual error plotted in

red is offset by 0.001 in order to clearly visualize the difference between the two

variables.
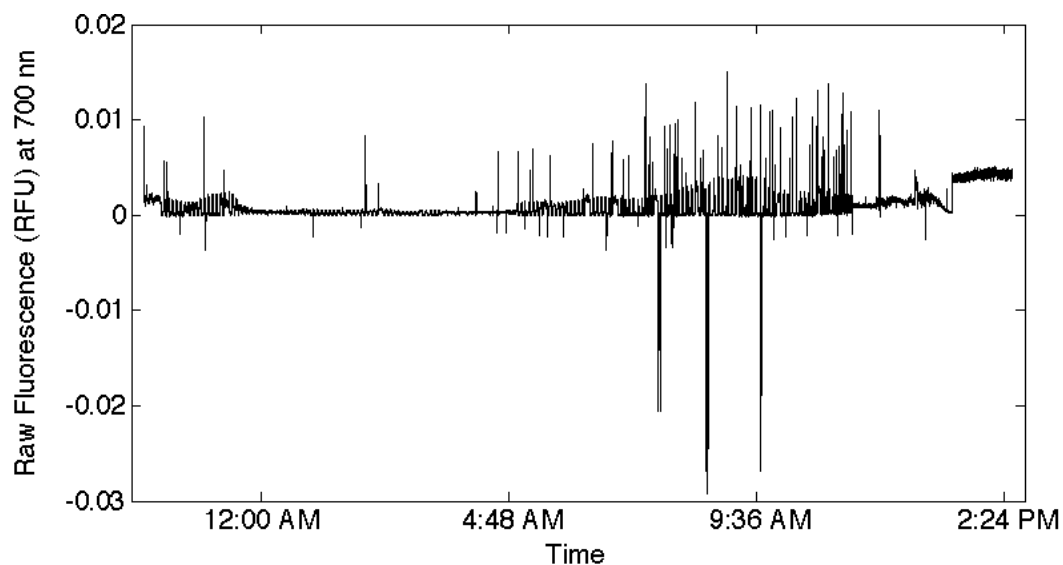
Figure 5. Raw fluorescence data at 700 nm with time for *Dorado* 150: May 29-30, 2012. Fluorescence values are raw data from the HydroScat fluometer.

Figure 6. Raw fluorescence at 700 nm with time for *Dorado* 150: May 29-30, 2012. NaN values and negative values removed are (in black), showing the spikes removed (in red) for analysis and comparison to PSD reconstruction.

Figure 7a. Fluorescence at 700 nm, PSD reconstruction, and residual error for full time period of *Dorado* 150: May 29, 10:00 PM to May 30, 2012 11:58 AM. Vertical black lines designate the start and end periods for subsets of the data chosen by fluorescence intensities. Subsets 1 and 3 were chosen as periods of high, continuous fluorescence with time, while Subset 2 is characterized by low fluorescence values and fewer data points. The fluorescence signal for the full dataset is n=16550 data points.

Figure 7b. Fluorescence vs. PSD reconstruction for the full time period of *Dorado* 150: May 29, 10:00 PM to May 30, 2012 11:58 AM. The PSD reconstruction for the full dataset has a strong linear relationship to fluorescence, described by y = 0.99x+2E-5, R^2 = 0.8132, $p < 0.001$.

35

Figure 8a. Fluorescence at 700 nm, PSD reconstruction, and residual error for the first subset of *Dorado* 150: May 29, 10:00 PM to May 29, 11:43 PM. The fluorescence signal for this subset is n = 4312.

Figure 8b. Fluorescence vs. PSD reconstruction for the first subset of *Dorado* 150: May 29, 10:00 PM to May 29, 11:43 PM. The PSD reconstruction for the subset has a strong linear relationship to fluorescence, described by y = 1x+2.8E-6, R^2 = 0.78622, $p < 0.001$.

36

Figure 9a. Fluorescence at 700 nm, PSD reconstruction, and residual error for the second subset of *Dorado* 150: May 29, 11:43 PM to May 30, 4:54 AM. The fluorescence signal for this subset is $n = 1004$.

Figure 9b. Fluorescence vs. PSD reconstruction for the second subset of *Dorado* 150: May 29, 11:43 PM to May 30, 4:54 AM. The PSD reconstruction for the subset has no relationship to fluorescence, described by y = 0.59x+1.3E-4, R^2 = 0.046328, $p < 0.001$.

Figure 10a. Fluorescence at 700 nm, PSD reconstruction, and residual error for the third subset of *Dorado* 150: May 30, 4:54 AM to May 30, 11:58 AM. The fluorescence signal for this subset is *n*=1123.

Figure 10b. Fluorescence vs. PSD reconstruction for the third subset of *Dorado* 150: May 29, May 30, 4:54 AM to May 30, 11:58 AM. The PSD reconstruction for the subset has a strong linear relationship to fluorescence, described by y=1x+5.3E-6, R^2=0.81211, *p* < 0.001.
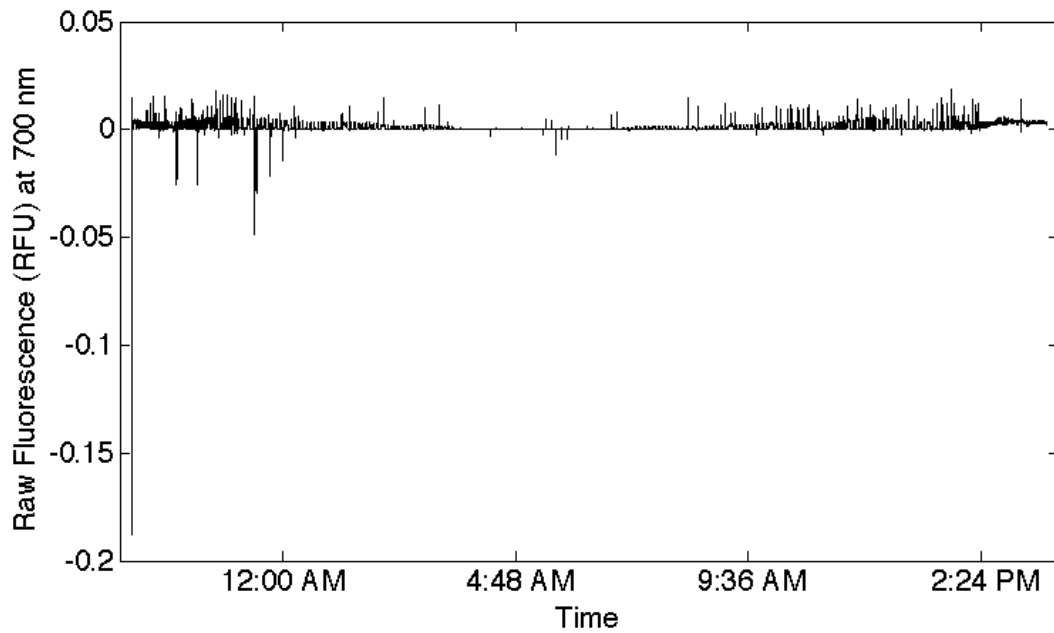
Figure 11. Raw fluorescence data at 700 nm with time for *Dorado* 151: May 30-31, 2012. Fluorescence values are from the Hydroscat fluometer.
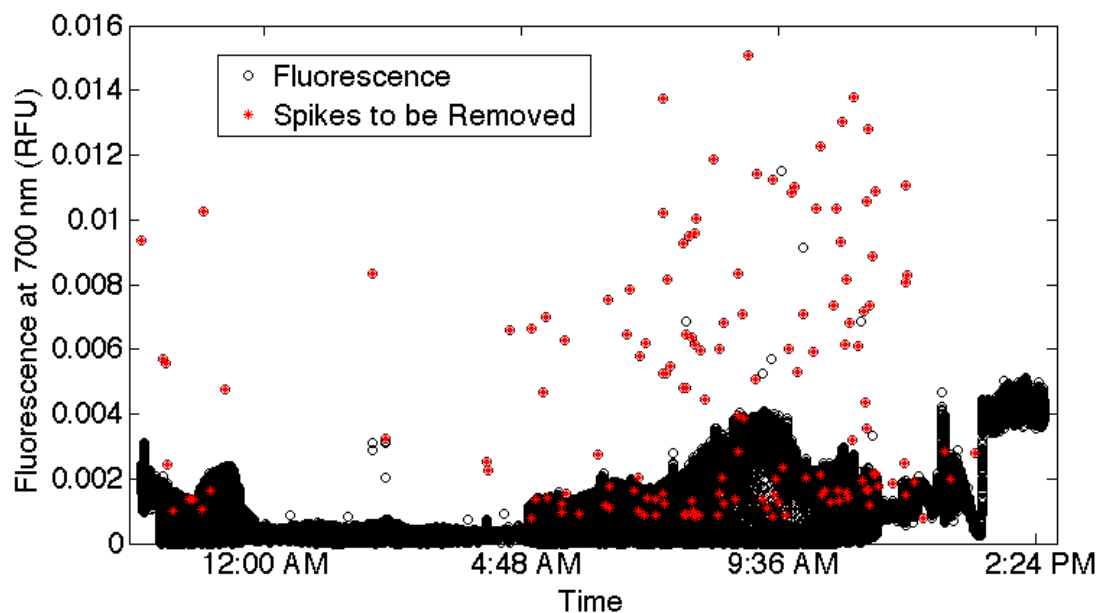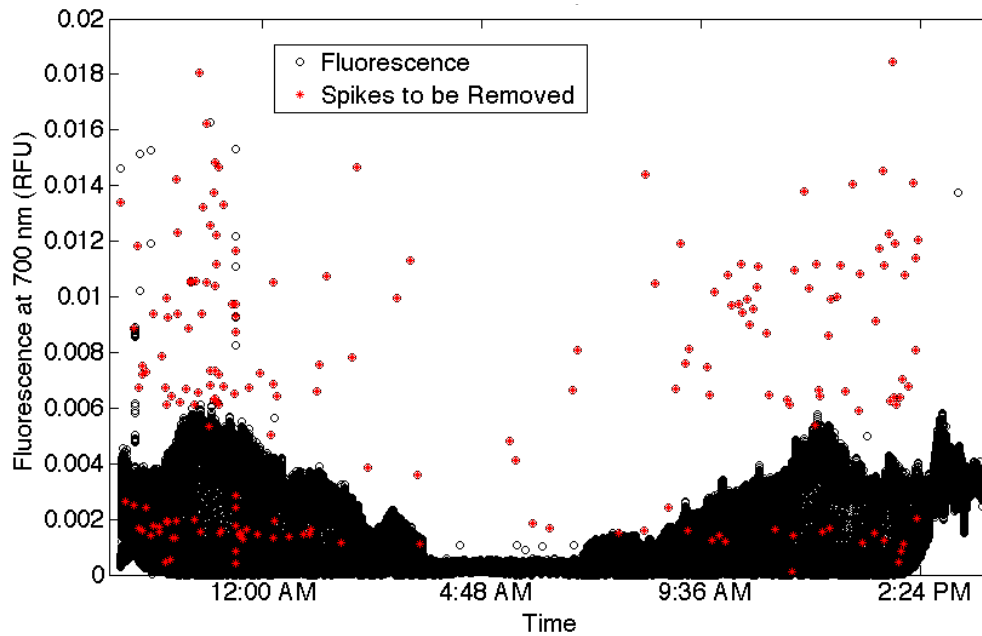

Figure 12. Raw fluorescence at 700 nm with time for *Dorado* 151: May 30-31, 2012. NaN and negative values are removed and data are shown in black. The spikes removed are in red.
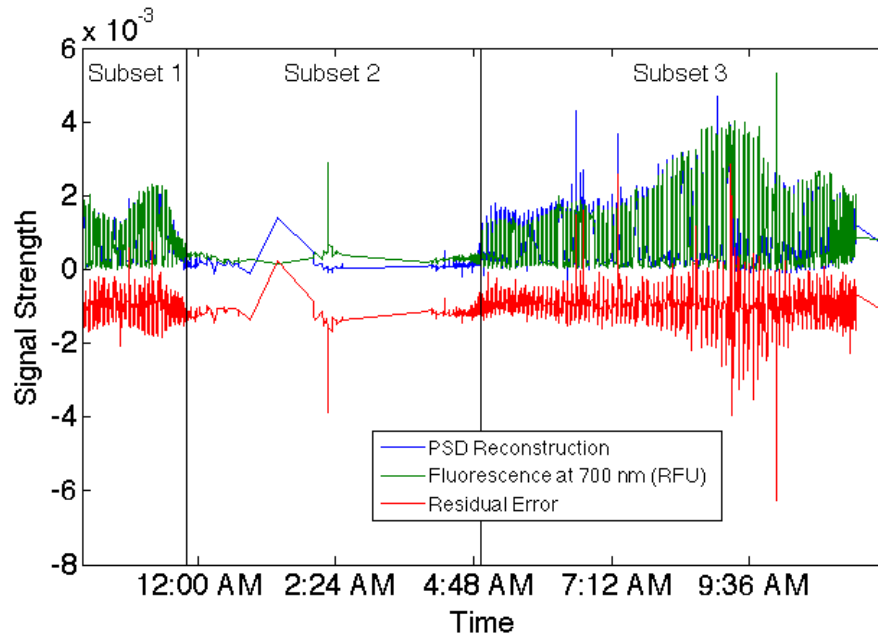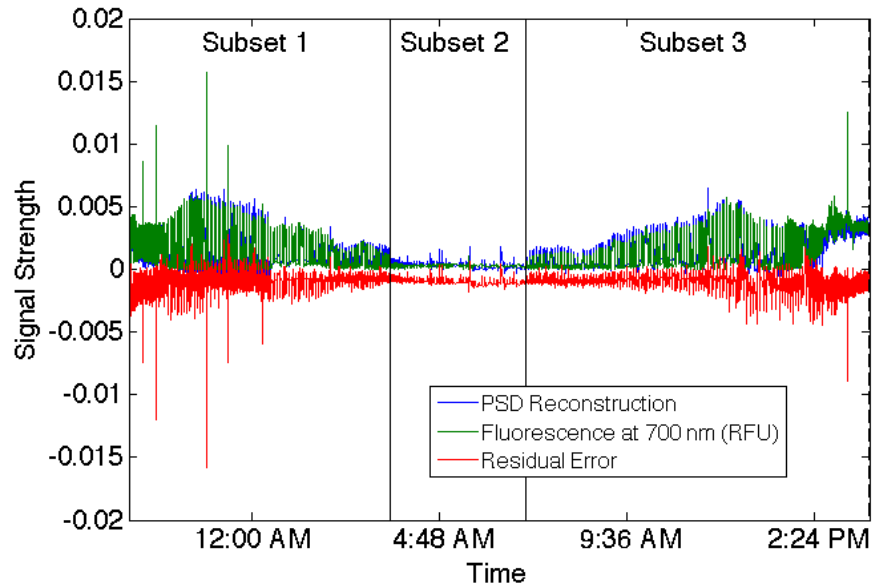
Figure 13a. Fluorescence at 700 nm, PSD reconstruction, and residual error for full time period of *Dorado* 151: May 30 8:53 PM to May 31, 2012 3:46 PM. Vertical black lines indicate the start and end periods for subsets of the data chosen by fluorescence intensities. Subset 2 contains fewer data points than Subsets 1 or 3, though unlike in Subset 2 of *Dorado* 150 (Fig. 9a), fluorescence values are continuous through the time period. The fluorescence signal for the full dataset is $n = 39227$.
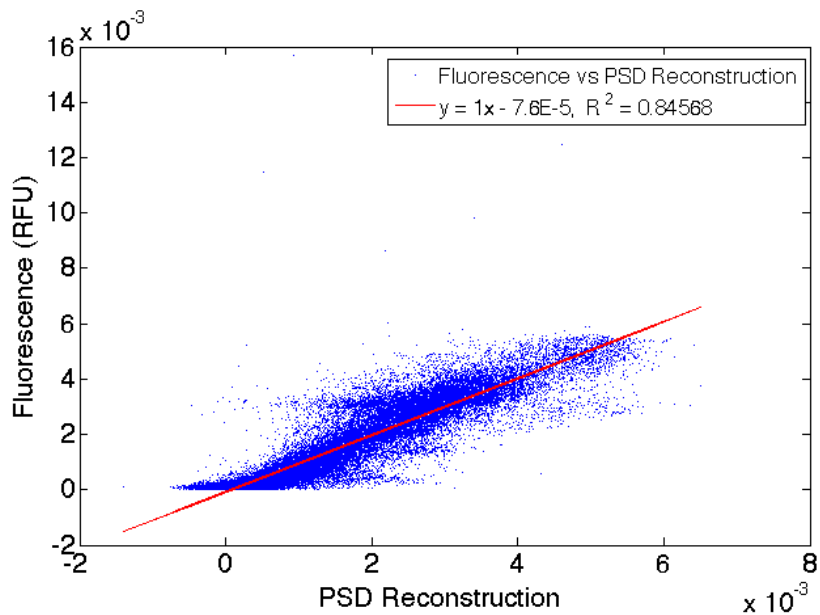
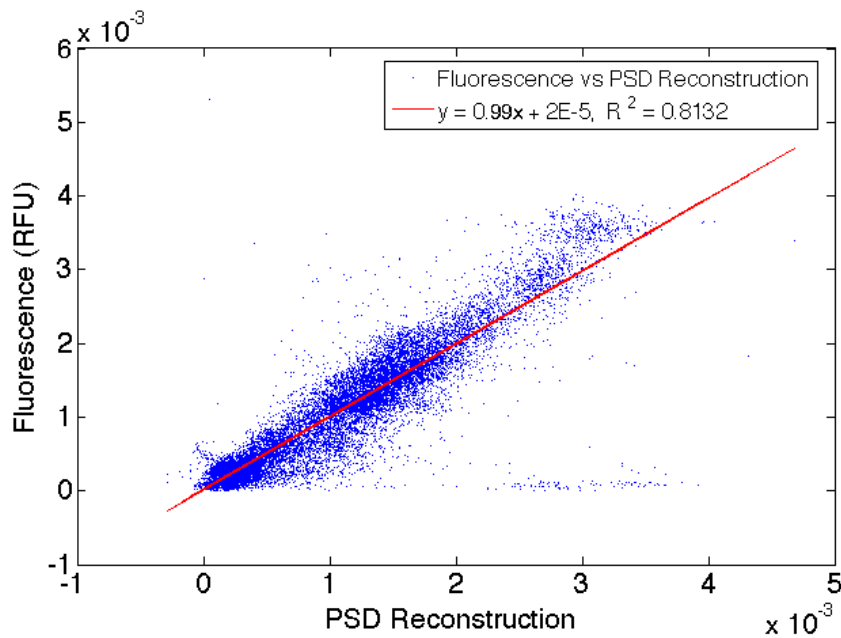

Fig 13b. Fluorescence vs. PSD reconstruction for the full time period of *Dorado* 151: May 30, 8:53 PM to May 31, 2012 3:46 PM. The PSD reconstruction for the full dataset has a strong linear relationship to fluorescence, described by $y = 1x-7.6E-5$, $R^2 = 0.84568$, $p < 0.001$.
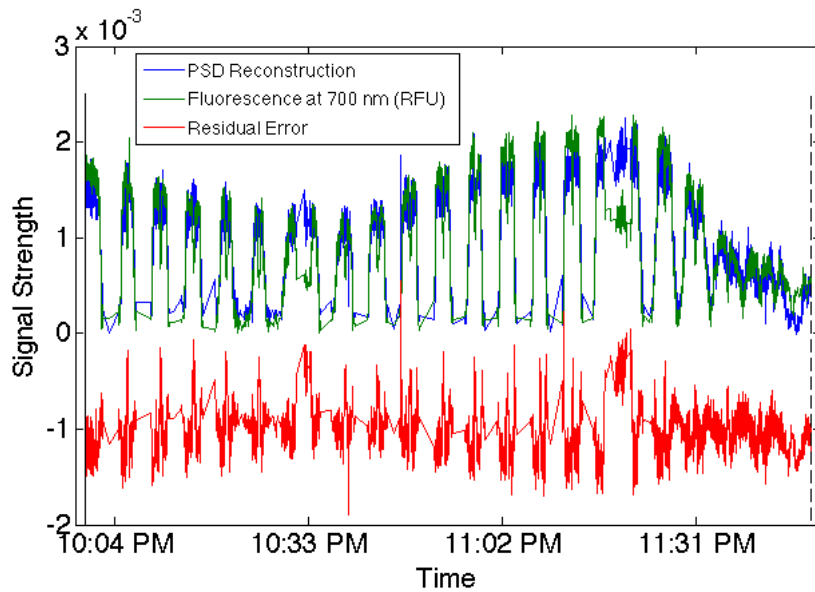
40
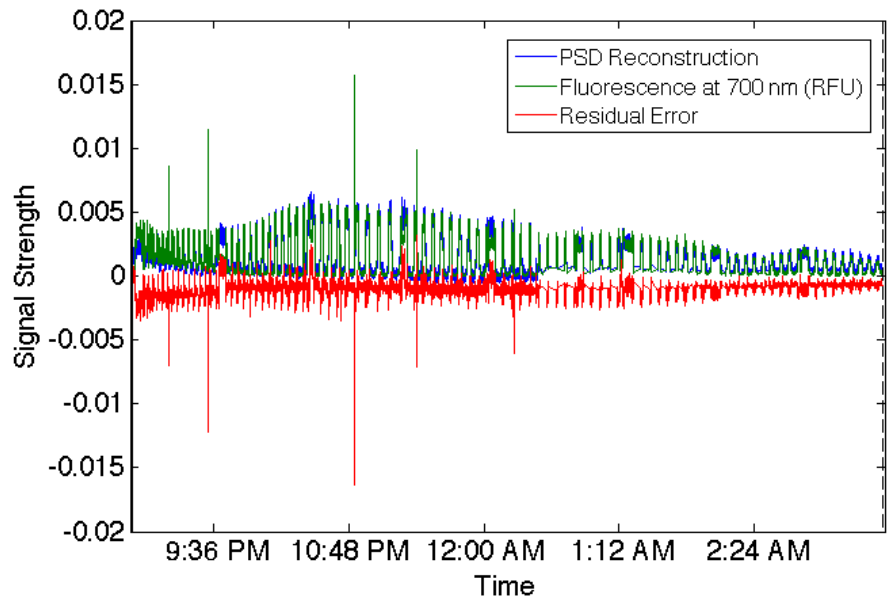
Figure 14a. Fluorescence at 700 nm, PSD reconstruction, and residual error for the first subset of *Dorado* 151: May 30, 8:53 PM to May 31, 3:32 AM. The fluorescence signal for this subset is *n* = 19062 points.
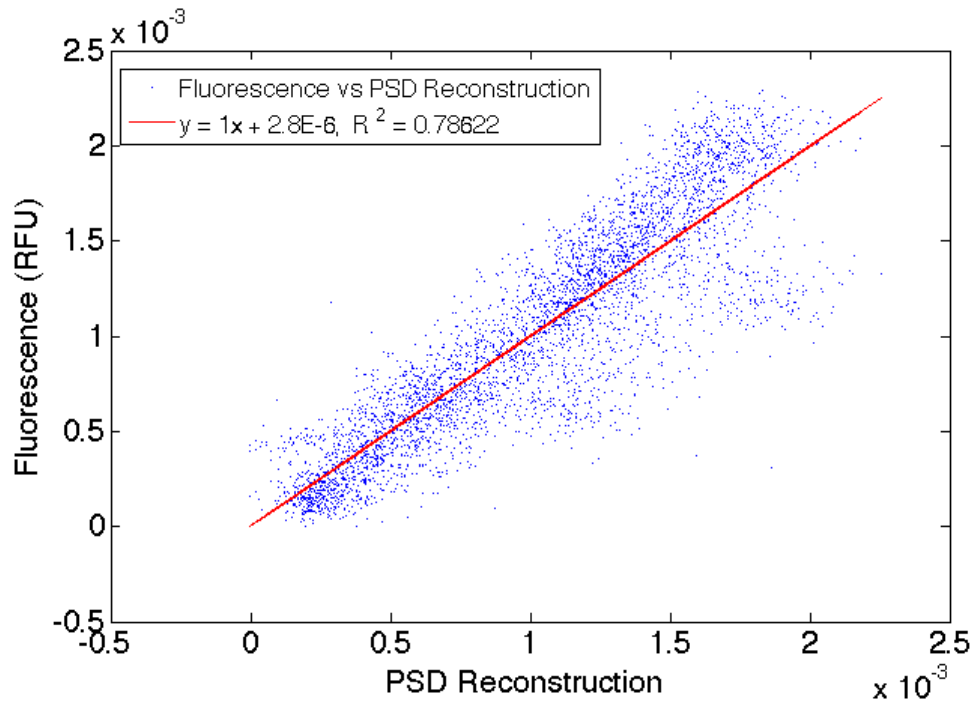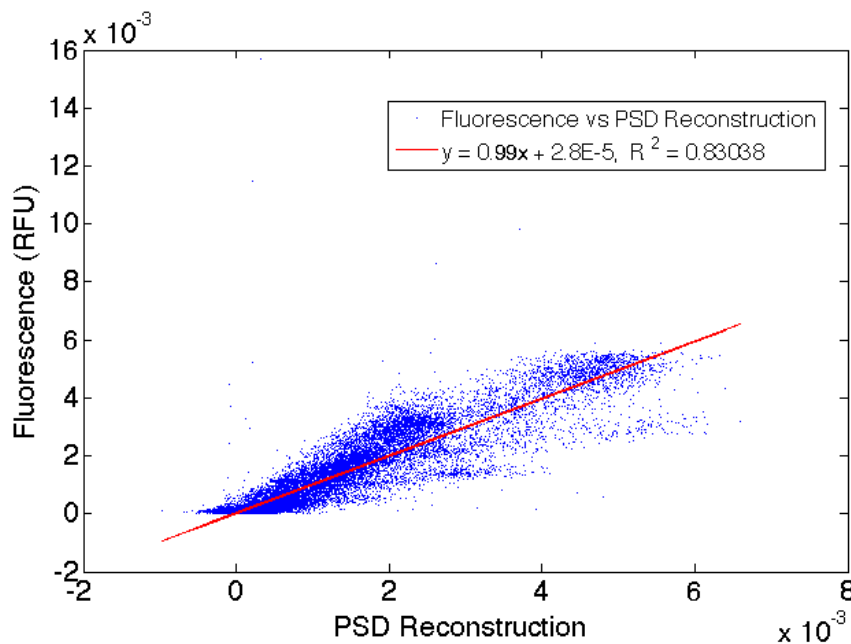

Figure 14b. Fluorescence vs. PSD reconstruction for the first subset of *Dorado* 151: May 30, 8:53 PM to May 31, 3:32 AM. The PSD reconstruction for the subset has a strong linear relationship to fluorescence, described by y = 0.99x+2.8E-5, R^2 = 0.83038, *p* < 0.001.
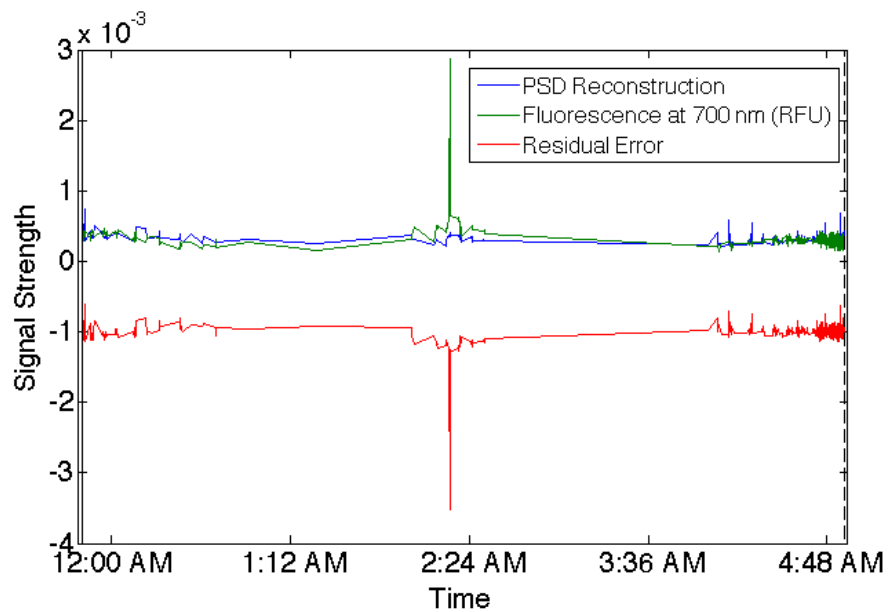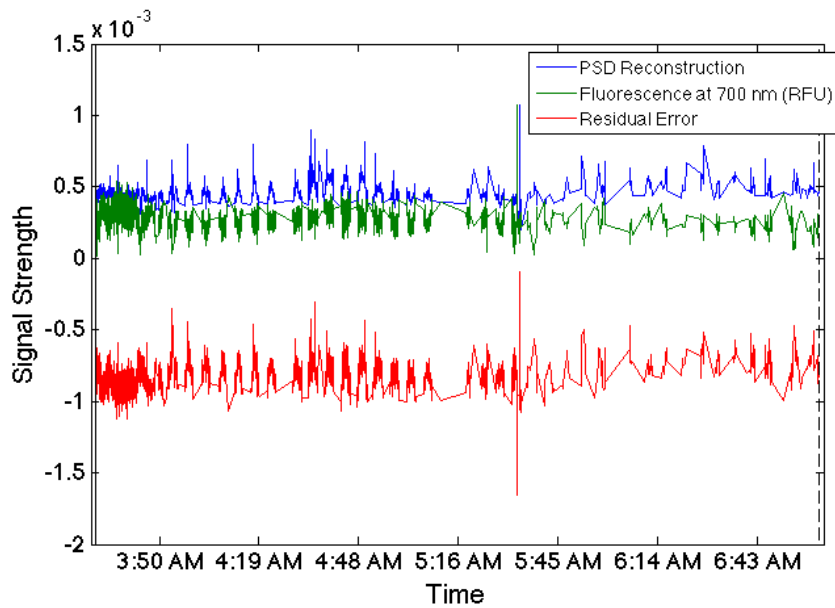
Figure 15a. Fluorescence at 700 nm, PSD reconstruction, and residual error for the second subset of *Dorado* 151: May 31, 2012 3:32 AM to May 31, 2012 07:00 AM. The fluorescence signal for the second subset is *n* = 3463 points.
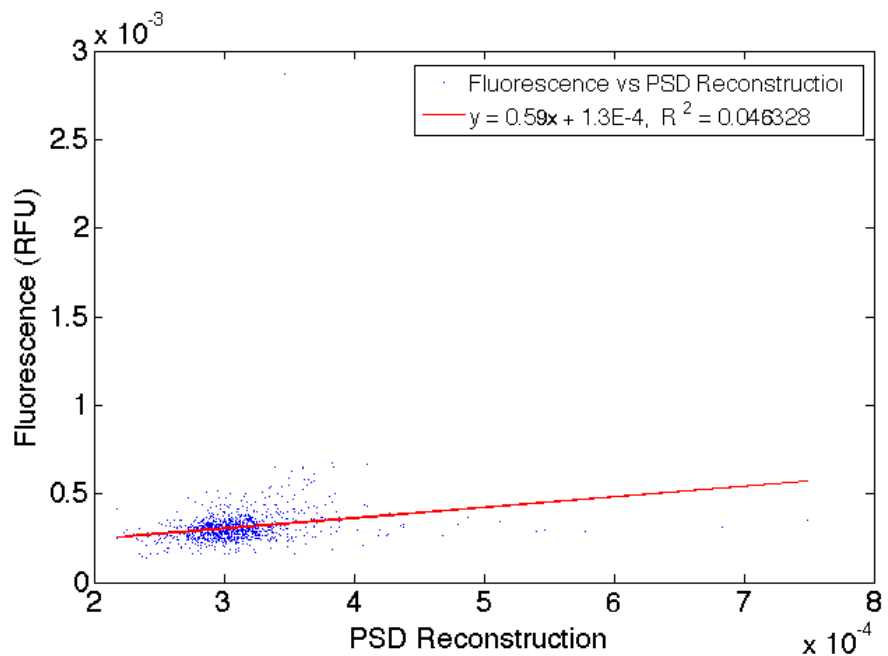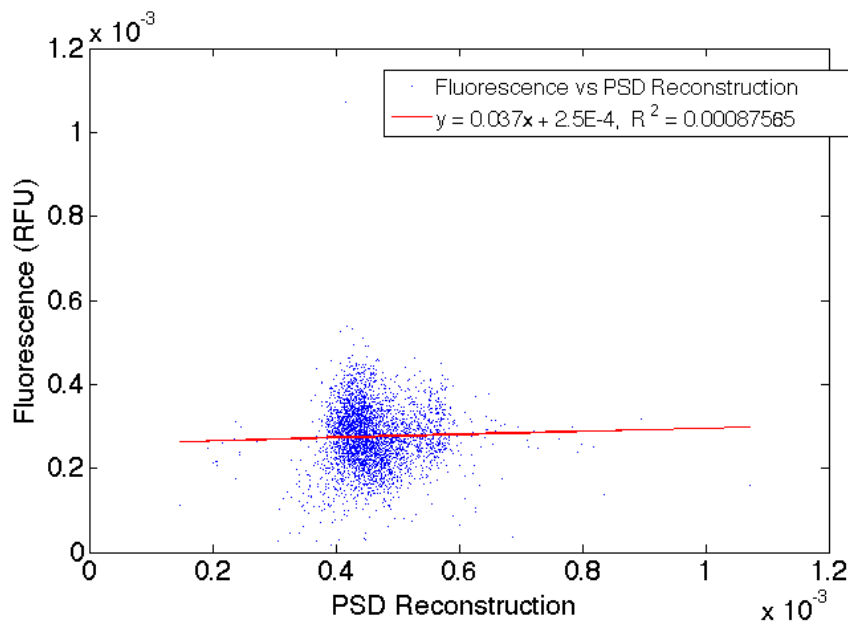

Figure 15b. Fluorescence vs. PSD reconstruction for the second subset of *Dorado* 151: May 31, 2012 3:32 AM to May 31, 2012 07:00 AM. The PSD reconstruction for the full dataset has no relationship to fluorescence, described by y = 0.037x+2.6E-4, R^2 = 0.00087565, *p* = 0.08.
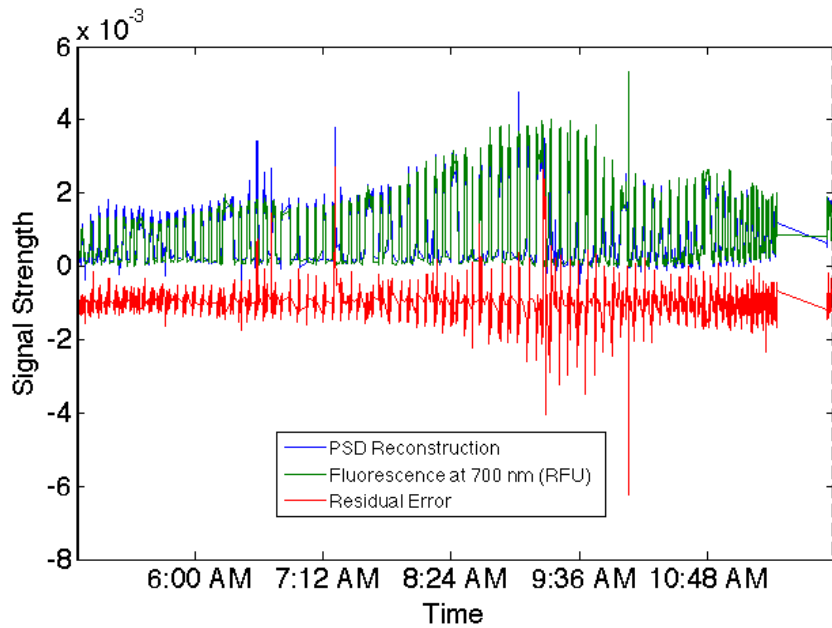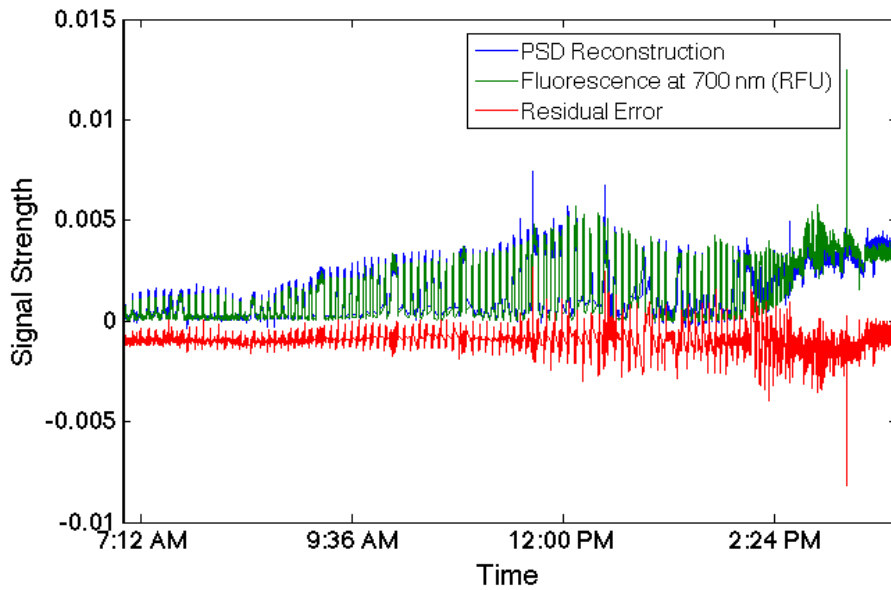
Figure 16a. Fluorescence at 700 nm, PSD reconstruction, and residual error for the third subset of *Dorado* 151: May 31, 7:00 AM to May 31, 3:46 PM. The fluorescence signal for the third subset is n = 16702 points.
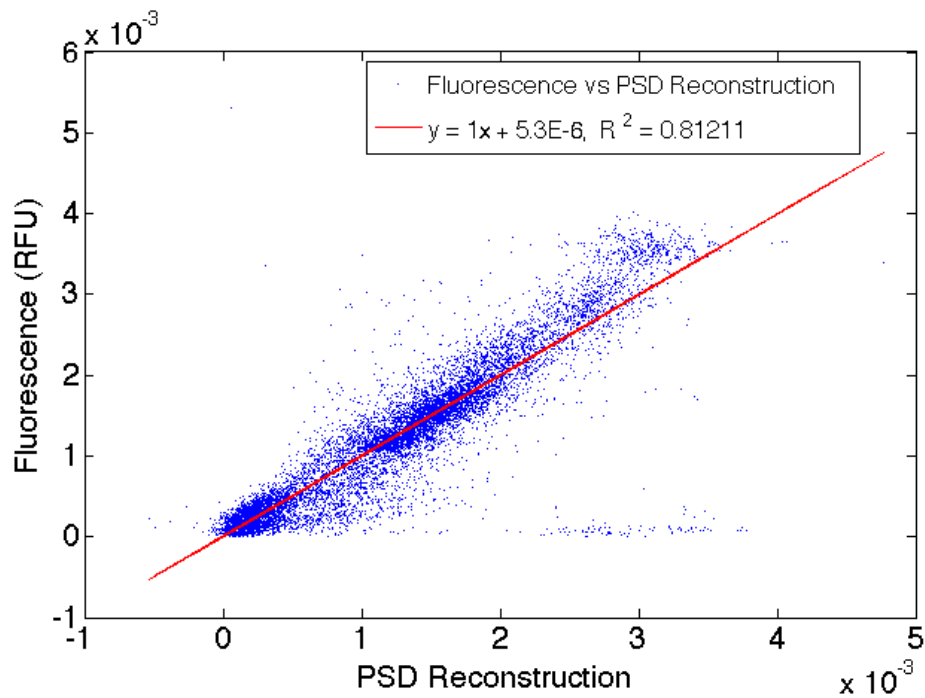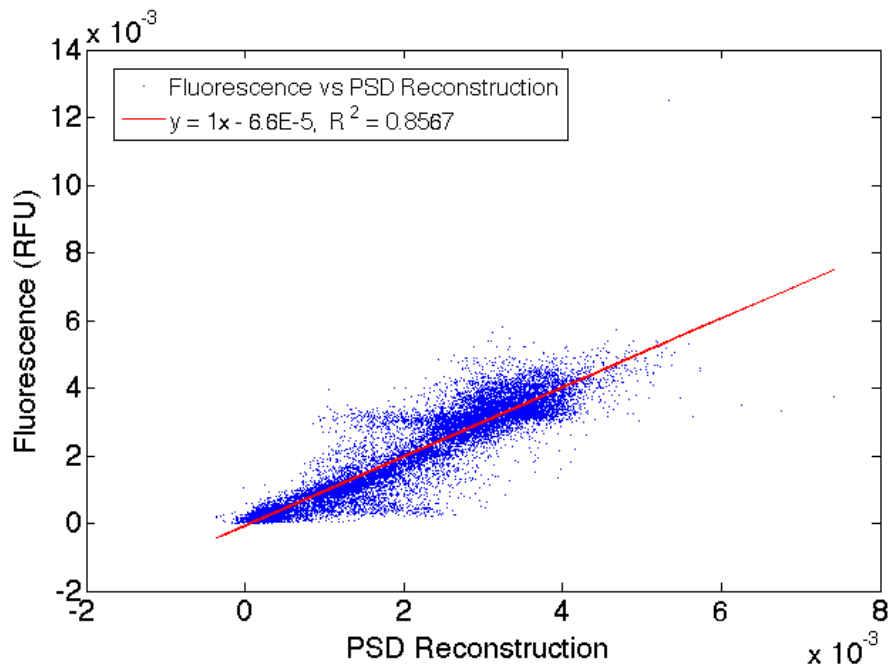

Figure 16b. Fluorescence vs. PSD reconstruction for the third subset of *Dorado*151: May 31, 7:00 AM to May 31, 3:46 PM. The PSD reconstruction for the subset has a strong linear relationship to fluorescence, described by y = 1x-6.6E-5, R^2 = 0.8567, p < 0.001.

The results indicate that *in situ* fluorescence can be closely replicated using a subset of LISST-100X forward scattering channels. The data show that different size classes dominate with different fluorescence intensities (Table 3). The reconstruction algorithm best fits the fluorescence data during periods of high and continuously recorded fluorescence values (Table 3, Figs. 8b, 10b, 14b, & 16b). The findings demonstrate the value of including particle size sensors on AUVs for studies in biological oceanography and plankton community dynamics.

In both the *Dorado* 150 and *Dorado* 151 datasets, the second subsets of fluorescence data were not well described by the PSD reconstruction ($R^2 = 0.046328$, $p < 0.001$ and $R^2 = 0.0008756$, $p = 0.08$) as demonstrated in Figs 9b and 15b, respectively. This could be due to the low quantity of fluorescence data points available relative to the other subsets. It is possible the fluorescence sensor was switched on and off overnight during the deployments to conserve power. Another possibility is that the sensor records a reduced number of values when it detects extended periods of low fluorescence.

By analyzing data from a subset of LISST-100X channels, a vehicle may be able to enhance adaptive sampling efforts by processing data faster than interrogating all 32 channels. The combination of channels used to reconstruct the fluorescence signal varies with the fluorescence values, indicating differing dominant particle sizes for different levels of fluorescence signal (Table 3). For data analyzed from the *Dorado* 150 mission, smaller size classes were associated with a lower fluorescence signal. In the case of the first subset of data, channel 14 dominated the PSD reconstruction, and in the second subset channel 7 dominated the reconstruction (Table 3). For the full datasets of each

mission, channel 20 dominated the PSD reconstruction (Table 3). These findings are encouraging for the ability of the LISST-100X to describe fluorescing biological organisms *in situ*. These results motivated the next section of this research, which investigates organism signatures for phytoplankton from an optical backscatter sensor and the LISST-100X forward scattering sensor.

3.2 Optical Backscatter Sensor Laboratory Tests, ECO Puck

The results from the 2012 optical sensor data analysis project inspired the interest in investigating the ability of forward and backscattering optical sensors to describe plankton in a controlled setting. This research seeks to address questions regarding the relationship between laboratory instrument counts of cell density and organism signatures in a controlled environment using two optical sensors that measure scattering. The laboratory instruments used to test these questions include the Accuri flow cytometer and Zeiss microscope with Sedgewick rafter. The two optical scattering sensors were the ECO puck optical backscattering sensor and the LISST-100X forward scattering sensor. This section details work performed in summer and fall 2013 using the ECO puck and monocultures of phytoplankton cultivated and tested in the laboratory at MBARI through the summer internship program, while the next section includes LISST-100X results and analysis.

The objective of the laboratory experiments using optical instruments and phytoplankton monocultures was to determine organism signatures and relationships to cell density determined in the laboratory. The experiments performed in this section

investigate the relationship between laboratory instrument counts of cell density and ECO puck chlorophyll concentration data for monocultures of phytoplankton. Five species of phytoplankton were cultivated and tested individually on the ECO puck sensor. Those species include *Micromonas sp.*, *Ostreococcus sp.*, *Heterosigma akashiwo*, *Pseudo-nitzschia heimii*, and *Pseudo-nitzschia australis*.

Investigating biological signatures with forward and backscatter sensors is valuable information for sampling large areas of the ocean over long time periods. Optical sensors mounted on an AUV demonstrate tremendous capability to describe physical and biological processes continuously in the ocean. When mounted on an AUV, the ECO puck can collect large quantities of data that can address questions about community processes and water composition over large spatial scales. Establishing a per unit chlorophyll cell density relationship provides applications in determining community structure from optical data. This experiment seeks to determine the relationship between chlorophyll concentration and cell density for of four species of phytoplankton tested as monocultures.

ECO puck backscatter for chlorophyll-α excitation at 470 nm is detected on the 695 nm emission wavelength detector. In this study the emission wavelength will be referred to for tables and figures, as the values are obtained from the 695 nm detector. The backscatter intensity values detected at 695 nm are corrected using laboratory-determined dark counts. Dark count values are obtained by covering the detectors only with black electrical tape, based on findings of Cetinić et al. 2009. Dark count results, as seen in Table 4, indicate that the ECO puck instrument is performing within the expected

range of the factory-calibrated dark counts. Chlorophyll concentration for excitation at 470 nm, in units of μg/L, is calculated from backscatter at the 695 nm detector using Equation 1. Provided by WET Labs, the "output" variable in Equation 1 is the backscatter intensity value from the ECO puck. Each "constituent" value, or chlorophyll concentration, determined in the laboratory is an average of 25 intensity measurements taken at a rate of 1.01 Hz over the course of about 30 seconds. The scale factor is a value provided by WET Labs and is specific to each wavelength and instrument.

$$[Constituent] = scale\ factor \times (output - dark\ counts) \qquad \text{(Equation 1)}$$

Determination of cell counts
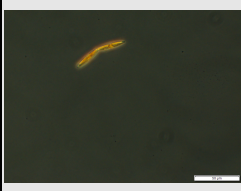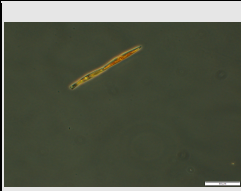
The laboratory cell counts data were obtained by flow cytometry or performing Sedgewick rafter counts of cells under a microscope. *Micromonas* counts performed using an Accuri flow cytometer in the Microbial Ecology (Worden) lab. *Heterosigma*, *P. heimii*, and *P. australis* counts performed using a Sedgewick rafter on a Zeiss Axioplan microscope, courtesy of the Worden and Scholin labs. The counting strategy used was based upon the size of the cell; cultures with cells below 5 um were counted on the flow cytometer, while the larger cells were counted via microscopy.

Cell densities for each monoculture tested were determined from cell counts and calculated as cells/mL. Those cell densities were multiplied by the volume of culture added to each experiment to determine the cell density for each increasing concentration of monoculture. Those values were then plotted against the chl-α values calculated using Equation 1, as seen in Figs. 17-21.

Table 4. Dark counts for the 695 nm wavelength for backscatter on the ECO Puck.

Date	λ	Scale Factor	WET Labs Dark Counts	Count	St Dev	Associated Organism Tests
31-Jul	695	0.0120	46	51.054	2.197	*Micromonas, Heterosigma*
27-Jan	695	0.0120	46	49.566	2.555	*P. heimii, P. australis*

Table 5. Monocultures cultivated in the laboratory.

Cell Image	Monoculture	Cell Size (µm)	Chl-density relationship (µg Chl/L/cell)
	Micromonas sp.	< 2	1E-5
	Heterosigma akashiwo	18-34	1.7E-3
	Pseudo-nitzschia heimii	30-100	1.37E-2
	Pseudo-nitzschia australis	50-100	2.3E-3

Average cell size and [chl] vs. density relationship calculations. Chl-density calculations are the slope for each monoculture experiment in Figs. 17, 20, and 21. Photo of *Micromonas sp.* by Deerinck, Terada, Obiyashi, Ellisman, &Worden (2009). http://www.mbari.org/news/news_releases/2009/micromonas/micromonas.html. Photo of *Heterosigma akashiwo*: Guiry, M.D. & WoRMS/Creative Commons (2013). Photos of *P. heimii* and *P. australis* by Diane Wyse/MBARI 2014

3.2.1 ECO Puck Sensor Data Analysis

The data for ECO puck show increasing chlorophyll concentration with increasing volume of organisms for all of the organism experiments (Figs. 17-21). In the five different monoculture experiments there is a linear relationship between the chlorophyll-α concentration and the calculated cell densities determined from laboratory counts (Figs. 17-21). Two laboratory tests were performed for separate monocultures of *Micromonas sp.* The chlorophyll concentration in Fig. 18 is approximately one order of magnitude lower than the values in Figure 17, but the relationship between cell density and chlorophyll concentration (slope=1E-5) is the same. The cultures were tested daily on a bench-top fluorometer to determine growth phase and health of the culture. The culture in Fig. 17 was tested on the ECO puck in the positive growth phase while the cells in Fig. 18 had passed positive growth and were less healthy. The difference in culture health is compared in Fig. 19, where the second less healthy *Micromonas* culture has lower cell density and chlorophyll concentration at each concentration of monoculture tested. It is important to note that the initial volume of culture tested in the second *Micromonas* sample is also lower, with a culture test volume range of 0.15 mL to 3 mL of culture in 600 mL of seawater, while the first culture has a test volume range of 0.3 mL to 12 mL in 600 mL of seawater. This difference was based upon the total volume of culture available to test on both the ECO puck and LISST-100X instruments.

Pseudo-nitzschia monocultures tested on the ECO puck were cultivated in the Scholin lab over the course of 3, 4, and 5 days. The *P heimii 1* and *P. australis 1* cultures in Figs. 22a-c were cultivated for 5 days (120 hours), *P heimii 2* and *P. australis 2* were

cultivated for 4 days (96 hours), and *P heimii 3* and *P. australis 3* were cultivated for 4

days (72 hours) in the Scholin lab 15ºC incubator on a 14:10 light/dark cycle. All

Pseudo-nitzschia monocultures were tested in the lab on the same day, over the course of

about three hours.

For analysis of results, data were collected, plotted, and analyzed in Microsoft

Excel, using the StatPlus add-on. The tests include linear regression analyses and

analysis of variance, or ANOVA, to determine the slope relationships between cell

densities and chlorophyll- α concentration for each sample.
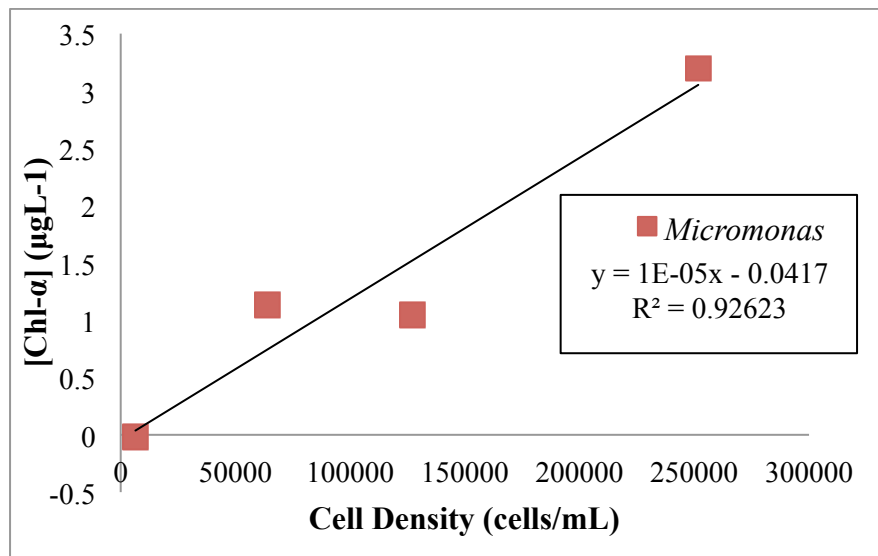
Figure 17. *Micromonas sp*. chlorophyll-α concentration at 695 nm with increasing cell density, 2 Aug. Measurements taken in filtered seawater on 2 Aug 2013. The relationship between the optical chlorophyll-α concentration and cell density is linear with a slope of 1E-5 µg Chl/L/cells/mL. A linear regression analysis with a one-way ANOVA shows a significant effect of cell density on chlorophyll concentration $p = 0.03$, $[F_{(2,1)} = 30.99]$.
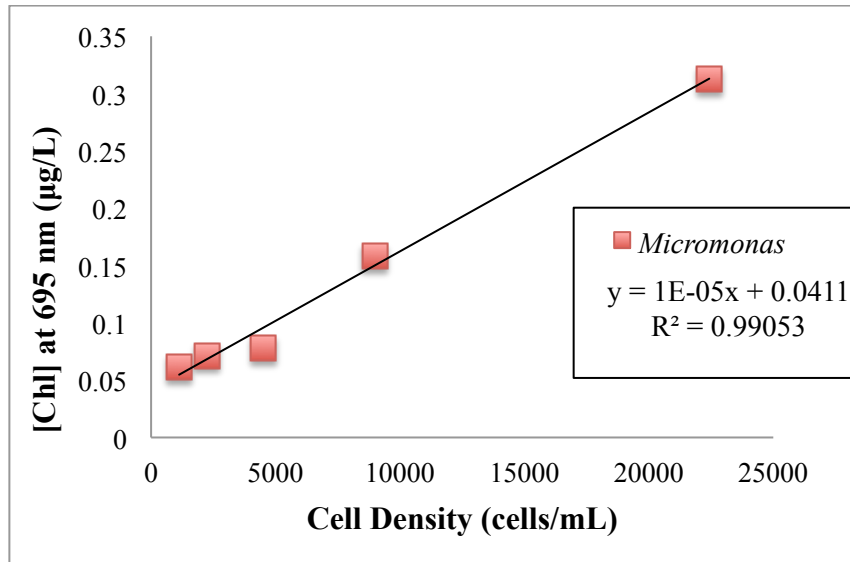
Figure 18. *Micromonas sp.* chlorophyll-α concentration at 695 nm with increasing cell density, 16 Jul. Measurements taken in filtered seawater on 16 Jul 2013. This plot shows the relationship between *Micromonas* cell density and chlorophyll concentration for low concentrations of chlorophyll. A linear regression analysis with a one-way ANOVA shows a significant effect of cell density on chlorophyll concentration $p = 0.004$, $[F(2,1)=211.83]$.
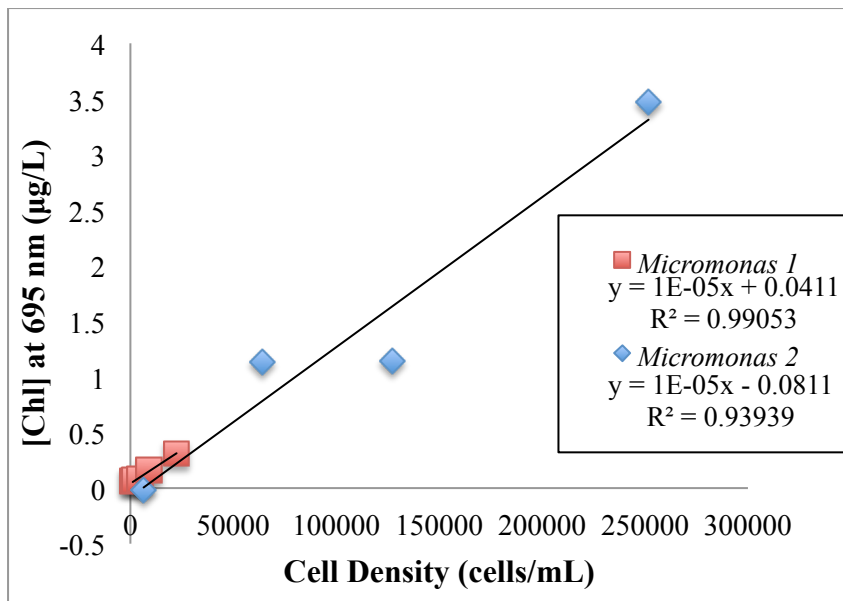
Figure 19. Chlorophyll-α concentration with cell density for two *Micromonas* samples (*Micromonas* 1: Jul 16, *Micromonas* 2: Aug 2, 2013). Samples from Figs. 17 and 18 plotted together to visualize relationships between lower and higher concentrations of sample. The relationship between chl-α concentration and cell density is linear in both cases, with a slope of 1E5 describing the relationship.
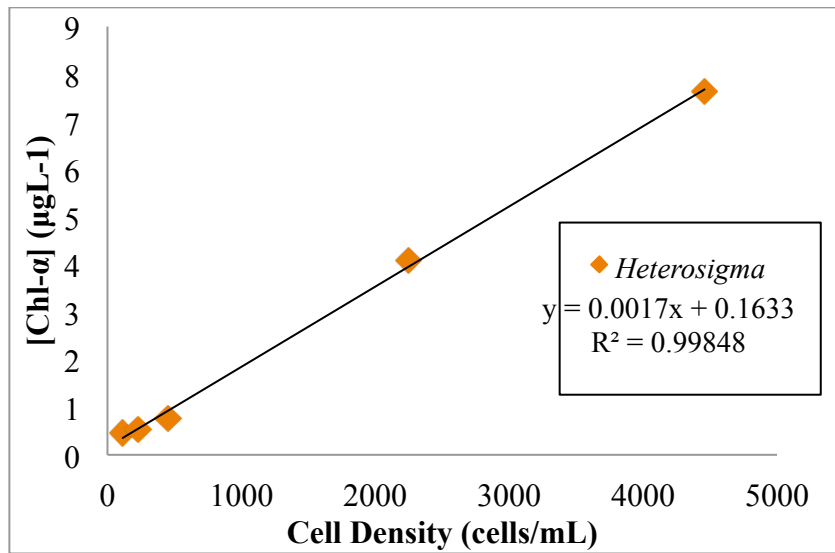
Figure 20. *Heterosigma akashiwo* chlorophyll-α density at 695 nm with increasing cell density. The relationship between the optical chlorophyll-α concentration and cell density is linear with a slope of 1.7E-3 μg Chl/L/cells/mL. A linear regression and one-way ANOVA shows a significant effect of cell density on chlorophyll concentration $p < 0.001$, [F(3,1) = 1.75E3].
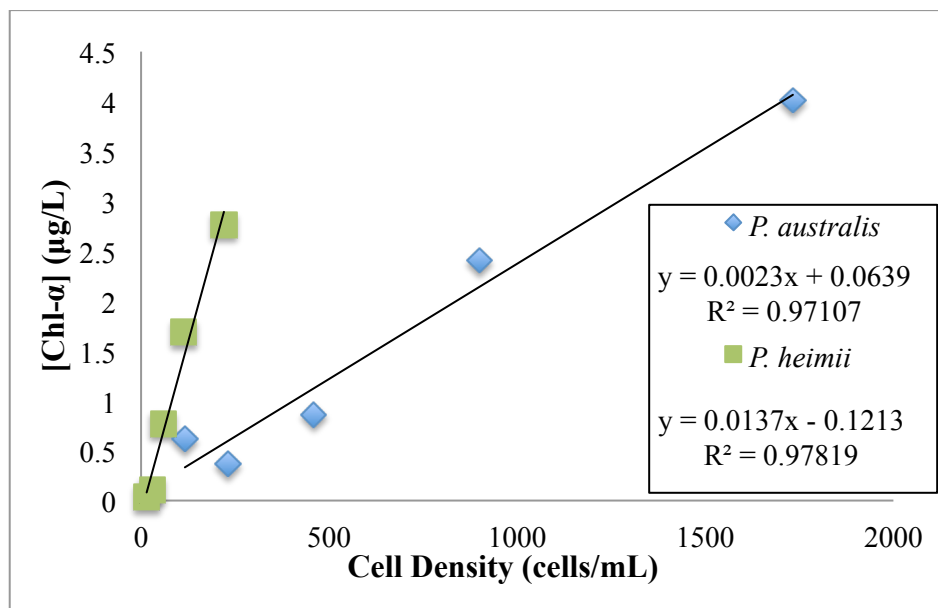
Figure 21. *P. heimii and P. australis* chlorophyll-α density at 695 nm with increasing cell density. The relationship between the optical chlorophyll-α concentration and cell density for *P. heimii* is linear with a slope of 1.37E-2 μg Chl/L/cells/mL. The relationship between chlorophyll-α concentration and cell density for *P. australis* is linear with a slope of 2.3E-3 μg Chl/L/cells/mL. A one-way ANOVA shows a significant effect of cell density on chlorophyll concentration for *P. australis, p = 0.02*, [F(3,1) = 100.7] and for *P. heimii, p = 0.001*, [F(3,1) = 134.5].

The different relationships between chlorophyll (chl-α) concentration and cell density for each of the monocultures can be explained by cell biology and size considerations. At a chl-α concentration of 3 μg/L, the smaller organism *Micromonas sp.* has about 300,000 cells (Fig. 17), while the larger organism *H. akashiwo* has approximately 1700 cells (Fig. 20). The vastly different cell densities at the same chl-α concentrations can be explained by the different cell sizes. *Micromonas* (<2 μm) is an order of magnitude smaller than *Heterosigma* (18-34 μm), so to achieve the same concentration of chlorophyll in an equivalent volume there would need to be many more *Micromonas* cells than *Heterosigma*. In the case of *P. heimii* and *P. australis* (Fig. 21), at 3 μg/L chl-α, the smaller and shorter chain-forming *P. heimii* has approximately 230 cells/mL, while the larger and longer-chain forming *P australis* has a culture density over 1200 cells/mL. Differences in cell densities could also be an indicator of culture health. Over the 120-hour incubation for the two *Pseudo-nitzschia* cultures in Fig. 20, the *P. australis* culture grew to be much more dense than the *P. heimii* culture.

To verify consistency for ECO puck data output with time, the size *Pseudo-nitzschia* tests performed on the same day were analyzed for intensity measurements made from the three detectors on the sensor. Each monoculture tested on the ECO puck and LISST-100X (discussed in the next section) took approximately half an hour to test. Data for the 470 nm, 650 nm, and 695 nm channels were processed using Equation 1 to convert from intensity counts to constituent concentrations. Figs. 22a-c show the relationship between the corrected scattering concentrations at each of the three

backscatter wavelengths ($\beta(117°, 470$ nm), $\beta(117°, 650$nm), and chlorophyll- α at 695 nm)

for all six *Pseudo-nitzschia* monocultures tested in the lab. The data in Figs. 22a-c

indicate consistency with time through the lab tests, from the first monoculture tested

through to the sixth test, and similar relationships between the backscatter data for each

species tested.
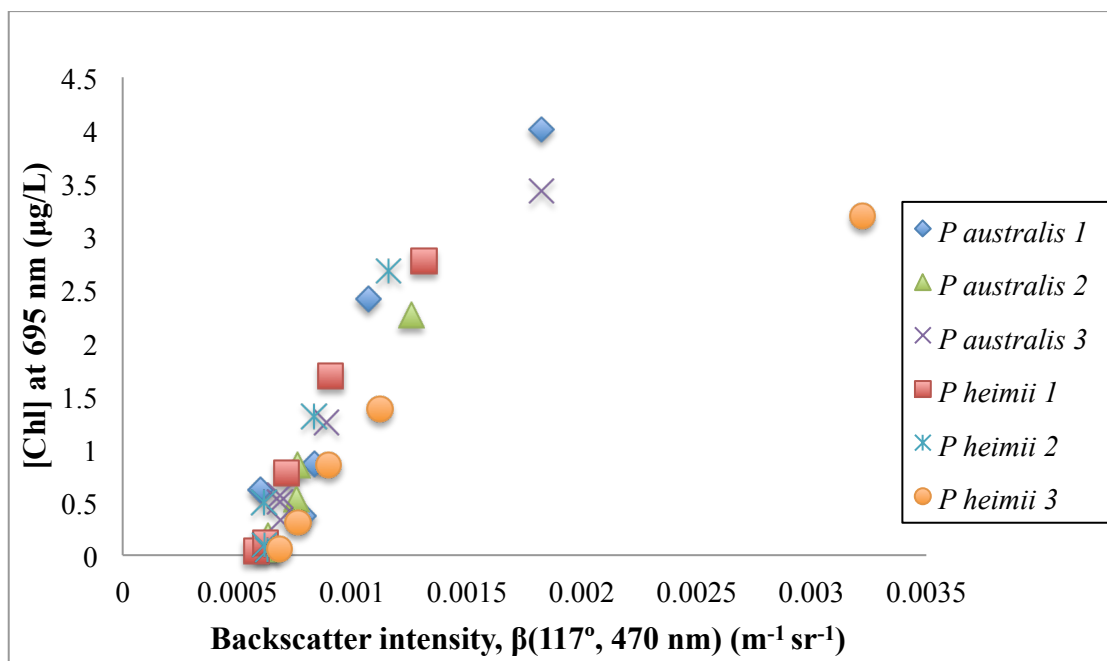
Figure 22a. Chl-α concentration at 695 nm. with $\beta(117°, 470$ nm) for 6 samples of
Pseudo-nitzschia. The data indicate a consistent relationship between backscatter at 117° and
chlorophyll concentration with each of the six experiments.
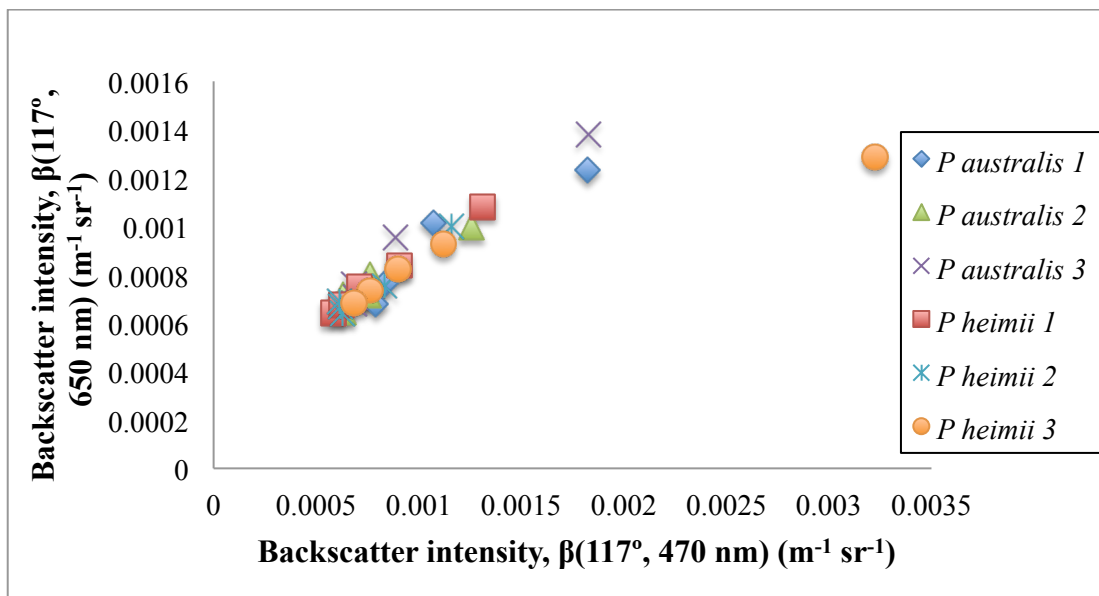
Figure 22b. Backscatter intensity at β(117º,650 nm) with β(117º, 470 nm) for 6 samples of *Pseudo-nitzschia.*
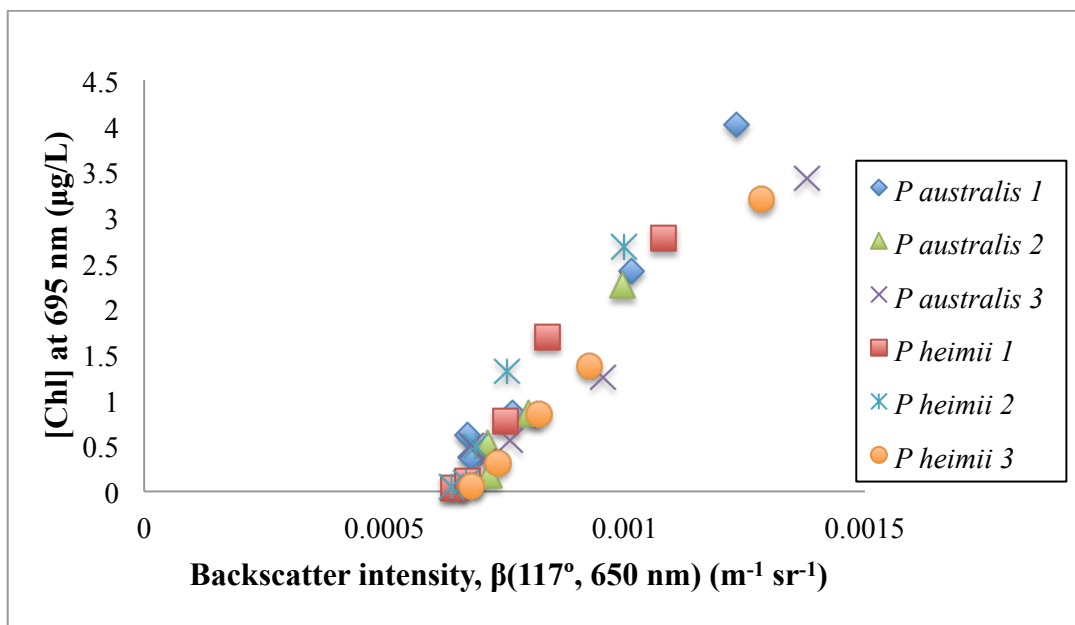
Figure 22c. Chl-α concentration at 695 nm with β(117º, 650 nm) for 6 samples of *Pseudo-nitzschia*

To investigate relationships between mean cell size and chlorophyll concentration per cell, the smaller cell-size (below 5 μm) monocultures were grouped and plotted in Figs. 23 and 24. The species in the small size group include *Micromonas sp.* and *Ostreococcus sp*. All three of the monocultures show a strong linear relationship between cell density and chlorophyll concentration (Fig. 23). A one-way ANOVA shows a significant effect of cell density on chlorophyll concentration for the 16 Jul *Micromonas* sample: $p = 0.004$, $[F_{(2,1)}=211.83]$, for the 2 Aug *Micromonas* sample, $p = 0.03$, $[F_{(2,1)} = 30.99]$, and for the *Ostreococcus* sample, $p = 0.001$, $[F_{(3,1)} = 107.8]$. Both of those monocultures were cultivated in the Worden lab and density counts were obtained using a flow cytometer.
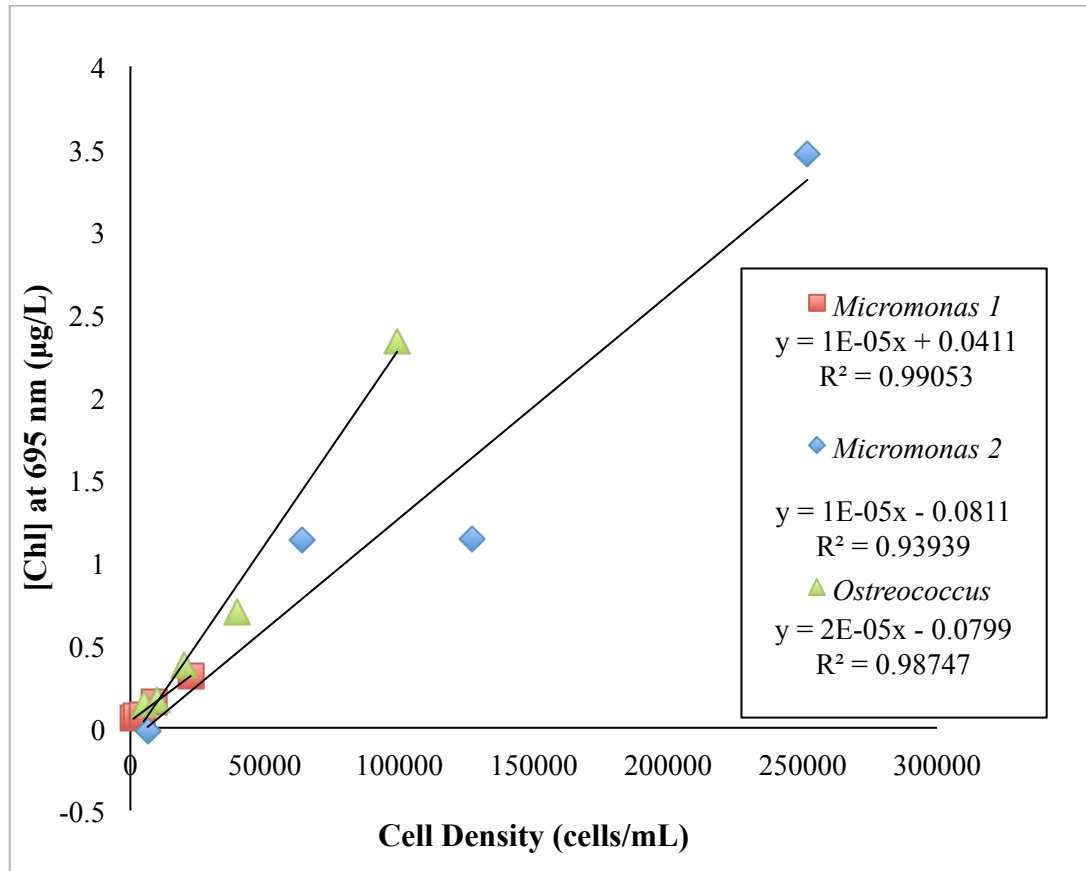
Figure 23. Monocultures with small cell sizes: chlorophyll concentration vs. cell density. Two monocultures of *Micromonas* and one culture of *Ostreococcus sp.* were tested in three different experiments, with results from the two *Micromonas* experiments in Figs.17 and 18. Cell density data is from flow cytometer counts. A linear regression analysis with a one-way ANOVA for *Ostreococcus sp.* shows a significant effect of cell density on chlorophyll concentration $p = 0.001$, $[F(3,1) = 107.8]$.

When grouped together to develop an intuition for a size-based, in addition to species-based determination of the relationship between cell density and chlorophyll, the three small-size class monocultures showed a strong linear and significant relationship, $R^2 = 0.90$, $p < 0.001$, $[F(13,1) = 121.3]$ (Fig. 24).
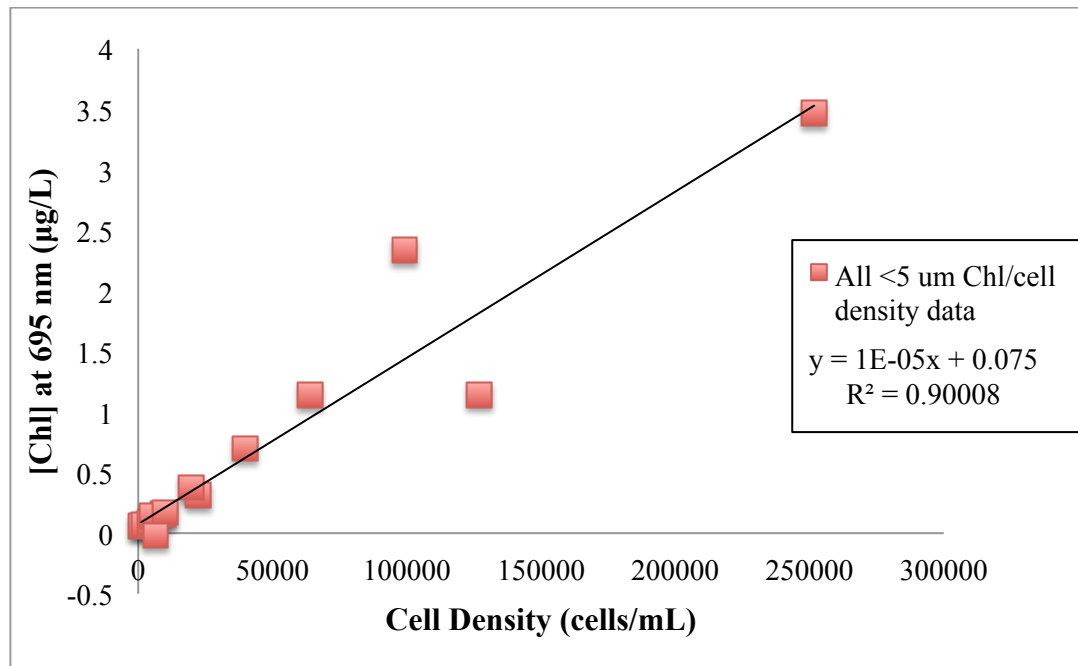
Figure 24. Chl-α concentration vs. cell density of all monocultures with small cell sizes, combined. Two monocultures of *Micromonas* and one culture of *Ostreococcus sp.* were tested in different experiments, with all data points grouped. Cell density data is from flow cytometer counts. The relationship between chlorophyll concentration and cell density for the grouped small cell data is 1E-5, with R^2=0.90008. A linear regression analysis with a one-way ANOVA for all small monocultures (< 5 μm) shows a significant effect of cell density on chlorophyll concentration $p < 0.001$, [$F_{(13,1)} = 121.3$].

Pseudo-nitzschia cultures were tested on the ECO puck and chlorophyll concentration vs. cell density was plotted for the three samples of each *P. heimii* and *P. australis* (Fig. 25). The data were then grouped by species (Fig. 26) and genus (Fig. 27). For a synthesized analysis of all monoculture tests based upon size, the slope of the lines and associated coefficient of determination values describing chlorophyll concentration vs. cell density for Figs. 17, 19, 20, and 25 were entered into Table 6 and plotted in Fig. 28.
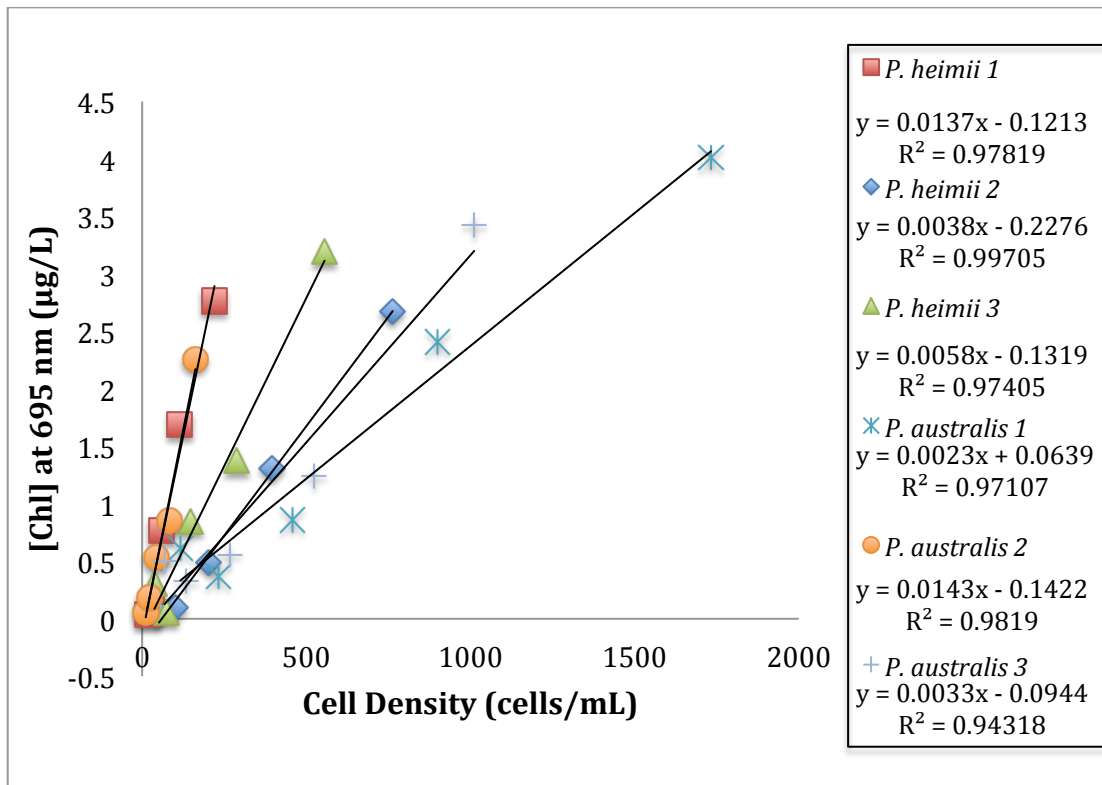
Figure 25. Chlorophyll concentration vs. cell density for the six *Pseudo-nitzschia* monocultures. Cell counts were performed using a Sedgewick rafter. The monocultures represent different incubation times, thus the range of cell densities from 10 to over 1000 cells/mL. This plot shows an increase of chl-α with increase in density for all cultures tested.

To determine the relationship of cell density to chlorophyll concentration for each *Pseudo-nitzschia* species tested the results were grouped by species and a linear regression analysis was applied to each species group. Chlorophyll concentration shows a strong linear relationship with cell density for both *P. australis* $p < 0.001$, $[F_{(13,1)} = 52.5]$ and *P. heimii* $p < 0.001$, $[F_{(13,1)} = 22.3]$ (Fig. 26).
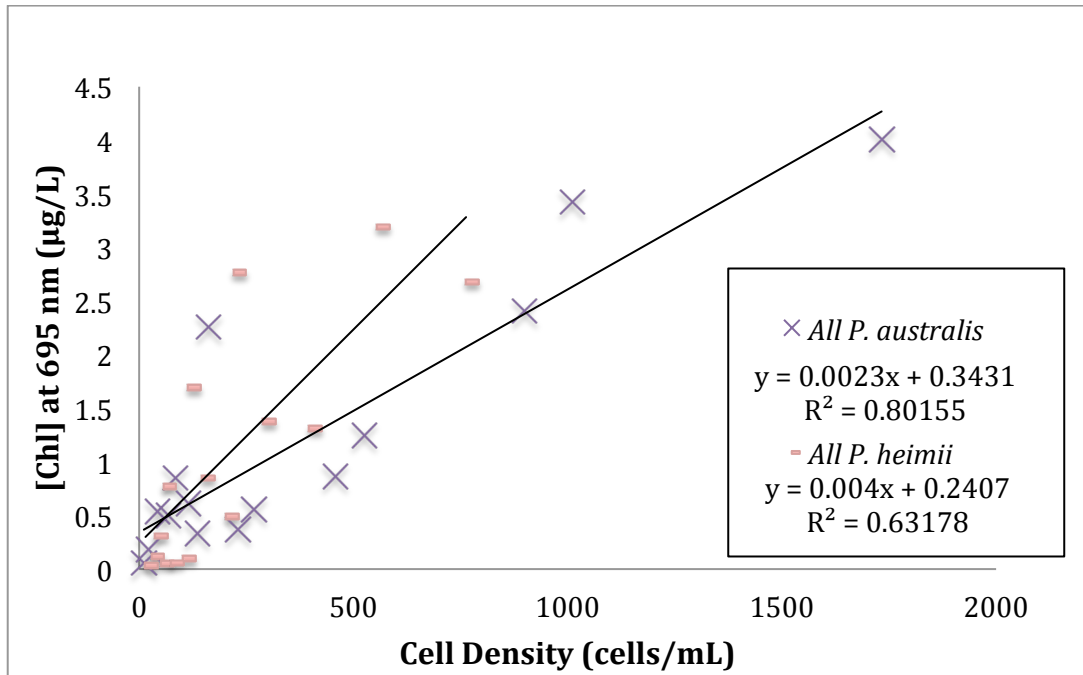
Figure 26. Chlorophyll-α concentration vs. cell density for the *Pseudo-nitzschia* monocultures grouped by species. Cell counts were performed using a Sedgewick rafter. The monocultures represent different incubation times, thus the range of cell densities from 10 to over 1000 cells/mL. This plot shows an increase of chlorophyll concentration with increase in density for all cultures tested, and a linear relationship for chlorophyll concentration vs. cell density for all samples within each species. A linear regression analysis with a one-way ANOVA for all *P. australis* shows a significant effect of cell density on chlorophyll concentration $p < 0.001$, $[F(13,1) = 52.5]$. A linear regression analysis with a one-way ANOVA for all *P. heimii* shows a significant effect of cell density on chlorophyll concentration $p < 0.001$, $[F(13,1) = 22.3]$.
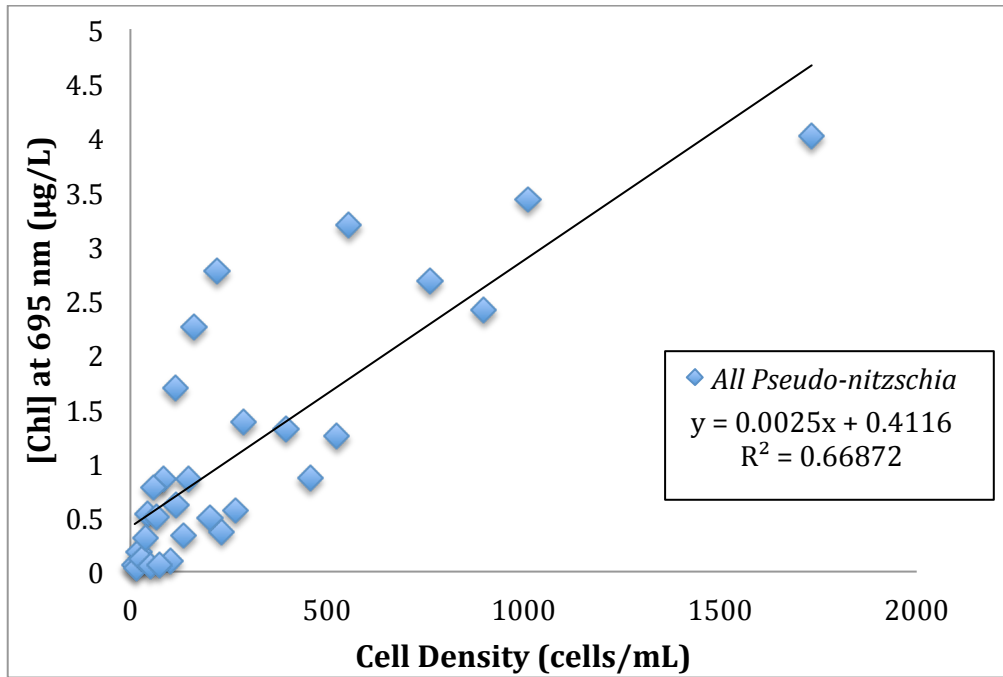
Figure 27. Chlorophyll concentration vs. cell density for all *Pseudo-nitzschia* tests. The slope of the chlorophyll concentration vs cell density relationship is 2.5E-3, indicating a linear relationship for all *Pseudo-nitzschia* samples collected, $R^2 = 0.668$. A linear regression analysis with a one-way ANOVA for all *Pseudo-nitzschia* tested shows a significant effect of cell density on chlorophyll concentration $p = 0.01$, $[F(28,1) = 56.5]$.

To compare the relationship between organism size and mean chlorophyll concentration per cell, the slopes describing the relationship of chlorophyll concentration vs. cell density for the monoculture experiments represented in Figs. 17, 19, 20, and 25 were entered into Table 6. The mean cell sizes, also in Table 6, were calculated using the high and low range for cell size and do not represent an exact mean for a distribution of all cells in a culture. The slope values presented in column two, in units of µg Chl-α/L/cells/mL, were divided by 1000 to convert milliliters to liters and calculate per cell chlorophyll concentration in units of µg Chl-α/cell (Table 6).

Table 6. Monoculture chlorophyll concentration vs. cell density relationships.

Species	[Chl- α] vs Cell Density (*m*)	R^2	Mean Cell Size /(μm)	Chl-a/cell = *m*/1000
Micromonas	1.00E-05	0.99053	1	1.00E-08
Ostreococcus	7.00E-06	0.97294	0.8	7.00E-09
Micromonas	1.00E-05	0.93939	1	1.00E-08
Heterosigma	1.70E-03	0.99829	20	1.70E-06
P. australis	2.30E-03	0.97107	75	2.30E-06
P. australis	1.43E-02	0.9819	75	1.43E-05
P. australis	3.30E-03	0.94318	75	3.30E-06
P. heimii	1.37E-02	0.97819	65	1.37E-05
P. heimii	3.80E-03	0.99705	65	3.80E-06
P. heimii	5.80E-03	0.97405	65	5.80E-06

Chlorophyll concentration vs. cell density values come from the slope the linear regression for the corresponding monocultures in Figs. 17, 19, 20, 25. Mean cell size represents and average of the range of cell sizes for each monoculture. Chlorophyll concentration per cell is calculated as the slope relationship in column two, divided by 1000 to convert mL to L for proper dimensional analysis.

In Figure 28, mean cell size is plotted against chlorophyll concentration per cell. The species represented include *Micromonas sp.*, *Ostreococcus sp.*, *H. akashiwo*, *P.australis,* and *P. heimii*. The cell size data are plotted with chl- α per cell to compare the relationship among multiple monoculture experiments. This grouping synthesis analysis was inspired by analysis performed in Perry & Porter (1989) in which absorption cross-section at 488 nm was plotted against flow cytometric chlorophyll-α for cells from cultures of 17 algal species.
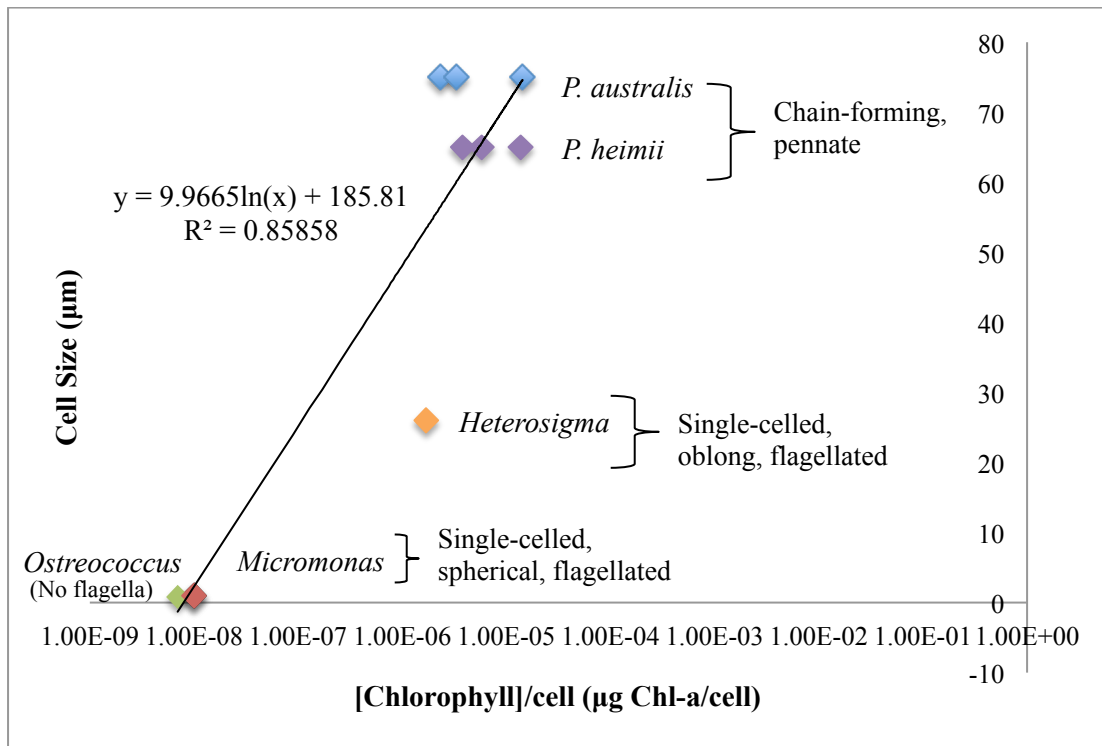
Figure 28. Mean cell size vs. chl-α per cell for all monoculture experiments. Chl-α per cell data are listed in Table 6. The chl-α data are calculated from ECO puck tests, and cell size data come from microscopy. The mean cell size for single-celled, spherical, flagellated *Micromonas sp.*is 1 μm, and 0.8 μm for *Ostreococcus sp.* The mean cell size for flagellated, oblong-shaped *Heterosigma* is 26 μm. Mean cell size for chain-forming, pennate *P. heimii* is 65 μm, and *P. australis* mean cell size is 75 μm. Mean cell sizes are an approximation calculated upon the high and low range for cell size and do not represent the exact mean for a distribution of all cells in a culture.

  The data show an expected difference in chlorophyll concentration per cell based upon mean cell size. *Pseudo-nitzschia* are larger cells than *Micromonas or Ostreococcus* and would be expected to have a greater concentration of chlorophyll in each cell. These results are comparable to work in Felip and Catalan (2000) which shows varying regression relationships between chlorophyll biovolume and cell size for different alga species from an oligotrophic mountain lake. While different conditions and species, both that study and this research show that the size and chlorophyll concentration of phytoplankton are important factors in understanding community composition through

optical methods. A test of other species with different cell morphology could supplement these findings to describe the relationship of mean cell size to chlorophyll concentration per cell across size classes between 5 μm and 30-100 μm.

3.3 Forward Scattering Sensor Laboratory Tests, LISST-100X

The objective of the experiments using the LISST-100X and phytoplankton monocultures was to determine organism signatures using particle scattering distributions. The experiments performed in this section investigate the volume concentration distributions from particle scattering for monocultures of phytoplankton. Four species of phytoplankton from three genera were cultivated and tested individually on the ECO puck sensor. Those species include *Micromonas sp.*, *Heterosigma akashiwo*, *Pseudo-nitzschia heimii*, and *Pseudo-nitzschia australis*.

The LISST-100X provides raw ring intensity counts and volume concentration distribution data for each test performed. Volume concentration distribution is obtained by performing an inversion of the raw ring intensity data using script provided by Sequoia Scientific, Inc. The following scripts were downloaded from the Sequoia website and run using MATLAB®.

getscat.m
tt2mat.m*
invert.p
vdcorr.m

* While available, the tt2mat script was not used for data processing because it performs a background reduction on the gain for DAT files. The LISST SOP software used to

collect data in this experiment saves data as ASCII and .log files, not binary DAT files. LISST-100X data saved in a DAT binary file includes a 10X gain.

The processed LISST-100X data show distinct differences in particle size and volume concentration distributions across the three genera tested. These experiments also show the expected result of an increase in volume concentration with increasing concentrations of organisms in the two experiments. The initial concentration for each of the organism samples is a subsample of the highest concentration of sample tested on the ECO puck. That is to say, 100 mL of the final test for each organism ECO puck experiment was measured using a graduated cylinder and added to the sampling chamber for the LISST-100X. This step was performed to have a point of comparison between the ECO puck optical backscatter and the LISST-100X forward scattering data for each monoculture tested.

For each LISST-100X test, 50 consecutive measurements were recorded and saved using the LISST-100X SOP software, over the course of approximately one minute. Those raw log data files were then imported to Matlab, inverted to determine particle scattering distributions using the Sequoia Scientific scripts provided above, and averaged to a single value for each concentration of each monoculture test. A second addition of monoculture was added to determine whether the scattering distribution signal was consistent with an increase in concentration.

The data are presented as particle scattering distributions, where the volume concentration of each of the 32 size bins, or channels, from 1.25 to 250 μm is represented on the x-axis with associated median particle size, provided by Sequoia Scientific, Inc.

Within each distribution plot, data for a low and high concentration of monoculture were included to determine if an increase in scattering signal (volume concentration) was associated with an increase in density of the culture. For all four species tested, the expected increase in volume occurred with an increase in cell density (Figs. 29, 31, 33, and 35). Following each particle scattering distribution plot is a scatterplot of the low and high concentrations tested for each species, performed to determine the numerical relationship between the two culture concentrations. The density increased by approximately 1.6 for the *Micromonas* sample, with a tighter fit to the slope at the lower volume concentrations (Fig. 30). Figure 32 shows a volume concentration ratio of 1.7 for the two concentrations tested, and a similar trend with better fit to the equation at the lower volume concentrations. When compared to the *Micromonas* and *Hetrosigma* experiments, the two *Pseudo-nitzschia* tests (Figs. 34 & 36) show more scatter around the slope between the two concentrations tested, with ratios of 1.4 and 1.7, respectively.

Figure 29. Volume concentration distribution of *Micromonas sp.* with median particle size for a low (2.55E5 cells/mL) and high (7.45E5 cells/mL) concentration of monoculture. The shaded gray area indicates the expected cell size from lab cell size and density determination, less than 2 μm. The data indicate an expected increase in signal with increase in concentration, and a signal within the expected (<2 μm) size range. The high volume concentrations above 100 μm are likely due to particulates from the artificial seawater in which the *Micromonas* monoculture was tested.

Figure 30. Comparison of PSD for two concentrations of *Micromonas sp.* Data represent the relationship between the 32 PSD channels for a low concentration of 2.5E5 cells/mL and a high concentration of 7.4E5 cells/mL. Linear regression analysis shows a significant relationship between the two concentrations, $p < 0.001$, $[F_{(30,1)} = 24.28]$.
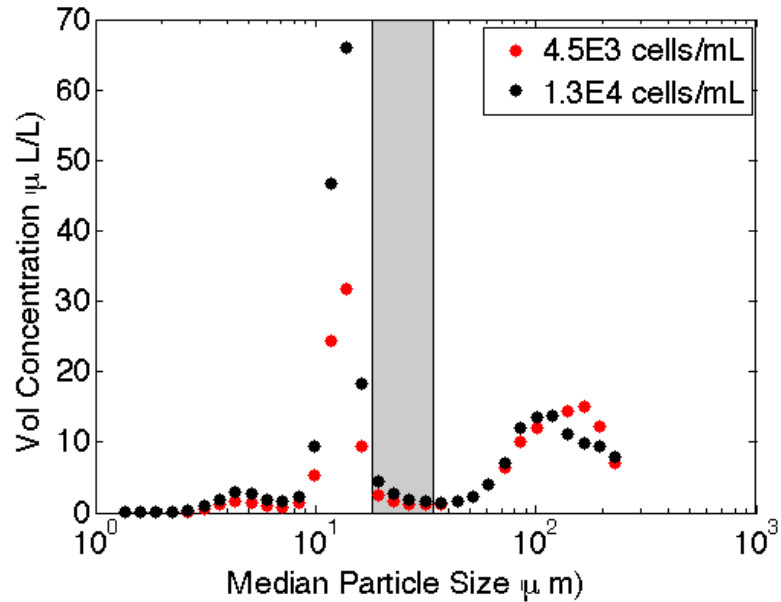
Figure 31. Volume concentration distribution of *H. akashiwo* with median particle size for low (4.53E3 cells/mL) and high (1.3E4 cells/mL) concentrations. The shaded gray area indicates the expected cell size from lab cell size and density determination, 18-34 μm. The data indicate an expected increase in signal with increase in concentration, and a signal approximately 10um below the expected size range. The volume concentration signal above 100 μm is likely due to particulates from the artificial seawater in which the *Heterosigma* monoculture was tested.
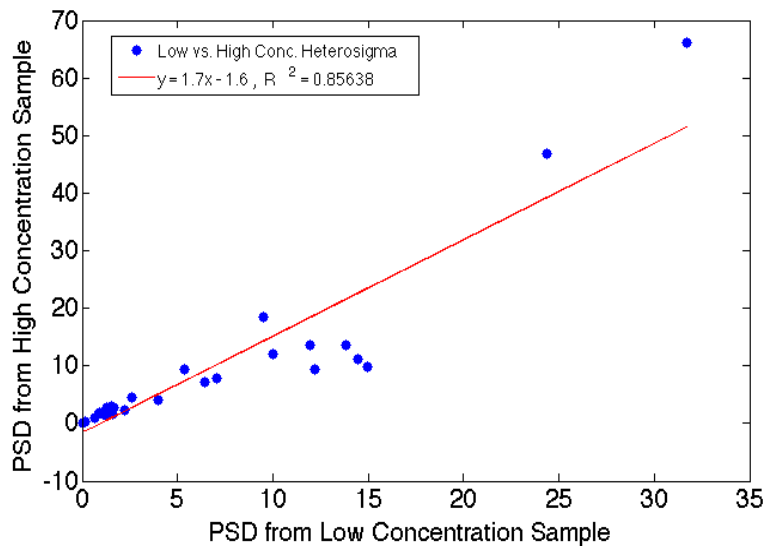
Figure 32. Comparison of PSD for two concentrations of *Heterosigma akashiwo*. Data represent the relationship between the 32 PSD channels for a low concentration of 4458 cells/mL and a high concentration of 1.3E4 cells/mL. Linear regression analysis shows a significant relationship between the two concentrations, $p < 0.001$, $[F(30,1) = 178.8]$.

The signal at the highest ring sizes for *Micromonas* and *Heterosigma* (Figs. 29 and 31) are much higher than expected given the mean particle size for *Micromonas* is two orders of magnitude lower, and the size range for *Heterosigma* is one order of magnitude lower. The unexpected peak in each of these two cases could be a product of background scattering from particulates in the filtered and autoclaved artificial seawater, or it could be the result of clumpy, dying cells. The two cultures were chosen in positive exponential growth, suggesting that the signal in the highest peaks is due to particulates in the filtered artificial seawater.
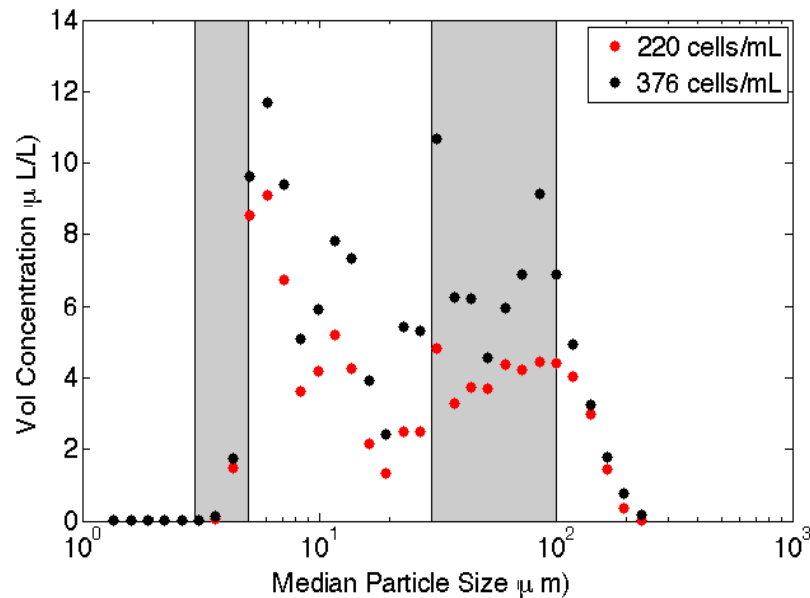
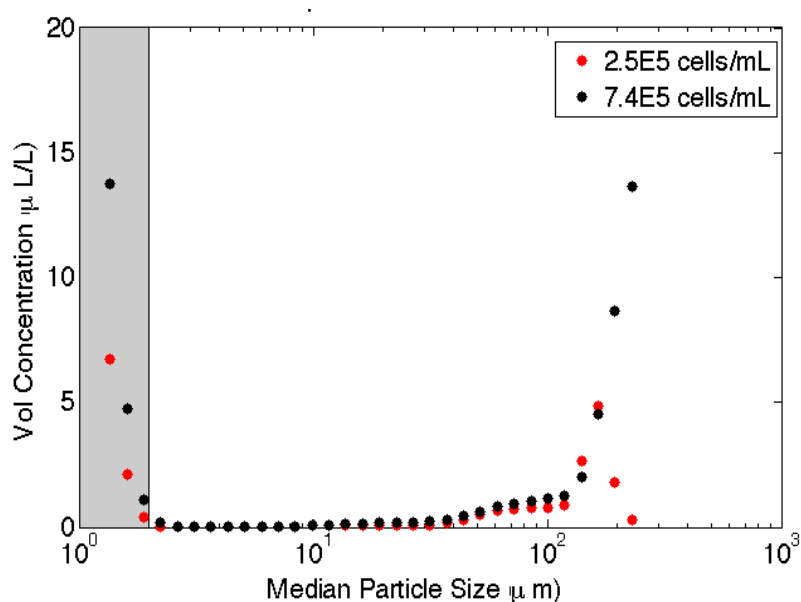

Figure 33. Volume concentration distribution of *P. heimii* with median particle size for a low (220 cells/mL) and high (376 cells/mL) concentration. The shaded gray area indicates the approximate expected cell width (3-5 μm) and length (30-100 μm) from lab cell size and density determined via microscopy. The data indicate an expected increase in signal with increase in concentration, and a peak within the expected size range.
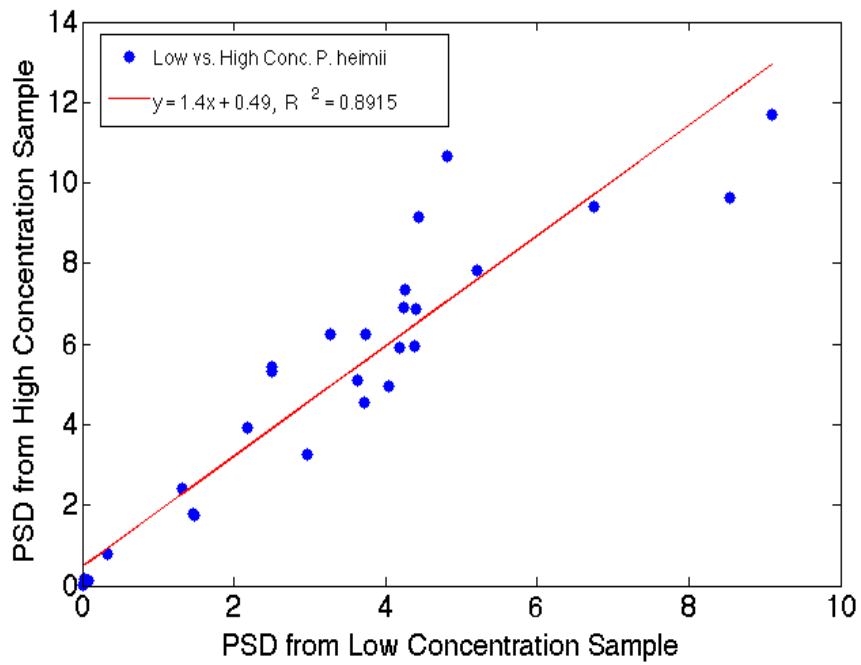
Figure 34. Comparison of PSD for two concentrations of *P. heimii*. Data represent the relationship between the 32 PSD channels for a low concentration of 220 cells/mL and a high concentration of 376 cells/mL. Linear regression analysis shows a significant relationship between the two concetrations, $p < 0.001$, [F(30,1) = 246.5].
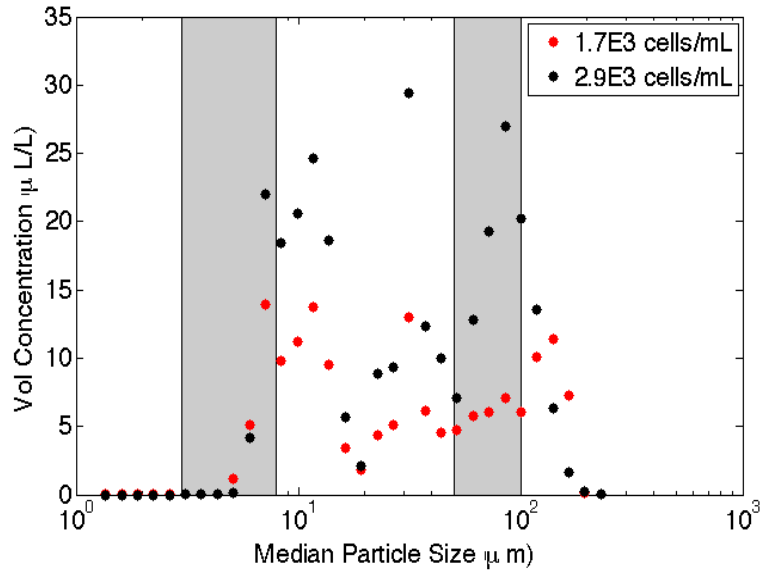
Figure 35. Volume concentration distribution of *P. australis* with median particle size for low (1.7E3 cells/mL) and high (2.9E3 cells/mL) concentration. The shaded gray area indicates the expected approximate cell width (5-10 μm) and length (50-100 μm) from lab cell size and density determined via microscopy,. The data indicate an expected increase in signal with increase in concentration, and a peak centered on the expected size range.
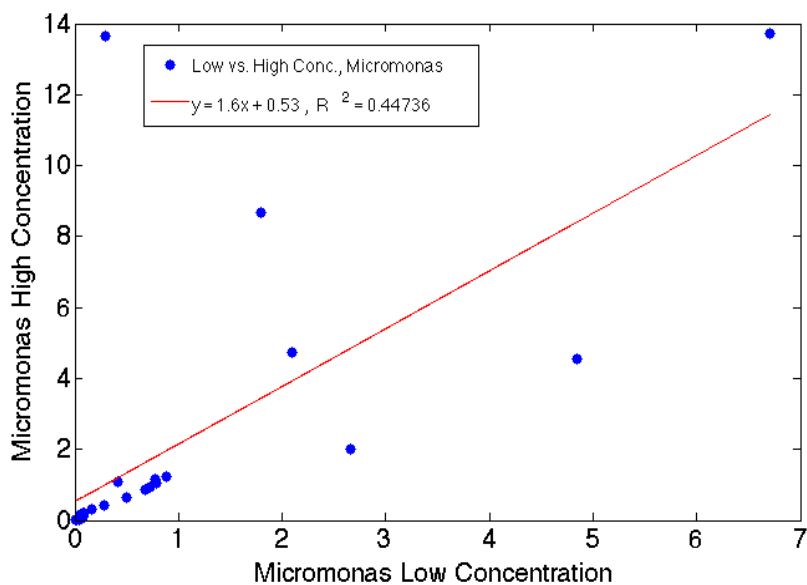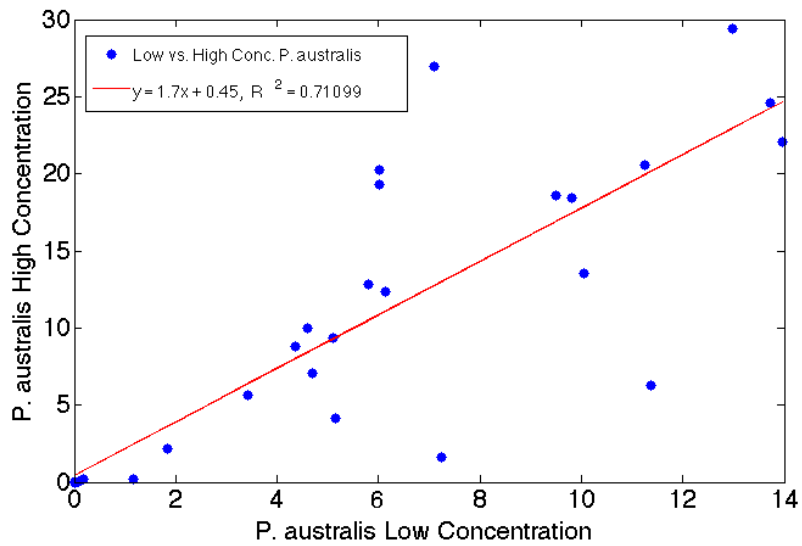

Figure 36. Comparison of PSD for two concentrations of *P. australis*. Data represent the relationship between the 32 PSD channels for a low concentration of 1.7E3 cells/mL and a high concentration of 2.9E3 cells/mL. Linear regression analysis shows a significant relationship between the two concetrations, $p < 0.001$, [$F(30,1) = 73.8$].

71

To test multiple samples of the chain-forming diatom, three cultures for each *P. heimii* and *P. australis* were cultivated in 5, 4, and 3-day increments. While the culture densities differed, the organism signature was consistent across all samples. In each *Pseudo-nitzschia* test there are two peaks, roughly centered around the width and length axes for the cells (Rienecker, et al. 2008). Figure 37 demonstrates the particle scattering distributions for six monocultures of *P. heimii* tested on the LISST-100X. Each experiment was incubated at 18ºC on a 14:10 light/dark cycle for 3, 4, or 5 days, as indicated in the legend. The low concentration is indicated in light green for the 5-day sample, light blue for 4-day sample, and gray for the 3-day sample. The higher concentration, approximately 1.7x more concentrated than the low concentration for the each incubation time, is indicated in the darker color corresponding to each sample. The volume concentrations with median particle size represent an average of fifty sample events taken over the course of a minute by the LISST-100X using the LISST SOP software. Experiments following the same methods were performed on *P. australis* (Fig. 38). The data follow a similar pattern to *in situ* and laboratory work performed by Rienecker et al (2008) for *Pseudo-nitzschia* samples in which one peak was recorded within the range of expected cell widths and another peak was recorded within the range of expected cell lengths, for a laboratory experiment and normalized *in situ* data during a *Pseudo-nitzschia* bloom.
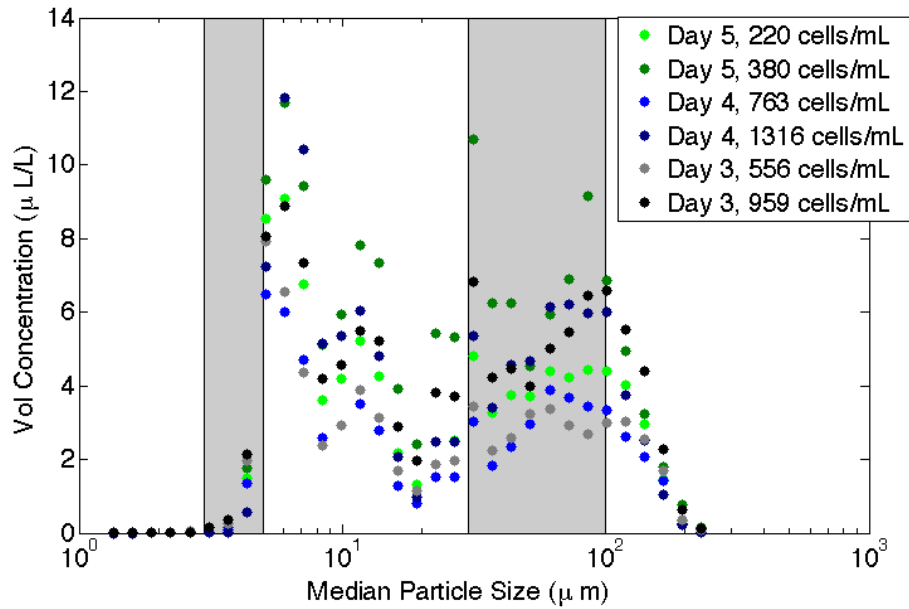
Figure 37. *P. heimii* volume concentration distributions with median particle size for cultures incubated for 5,4, and 3-days. Each incubation was tested at a low and high concentration. This plot shows a consistent signature pattern across the six concentrations tested. The gray bars indicate the expected cell width (3-5 μm) and length (30-100 μm) determined from microscopy.
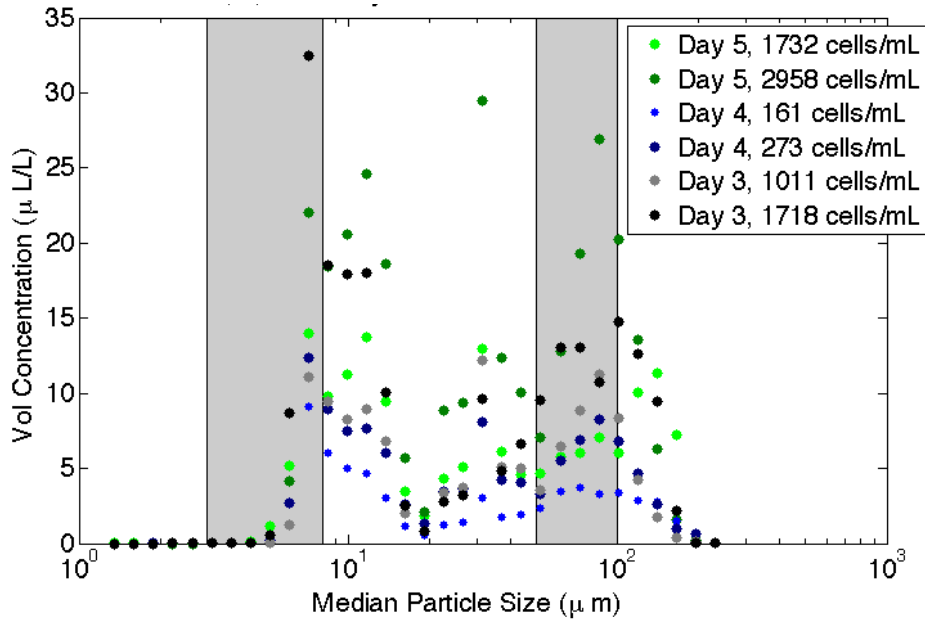
Figure 38. *P. australis* volume concentration distributions with median particle size for cultures incubated for 5,4, and 3-days. Each incubation period was tested at a low and high concentration. The data show a consistent signature pattern across the six concentrations tested. The gray bars indicate the expected cell width (3-8 μm) and length (50-100 μm) determined from microscopy.
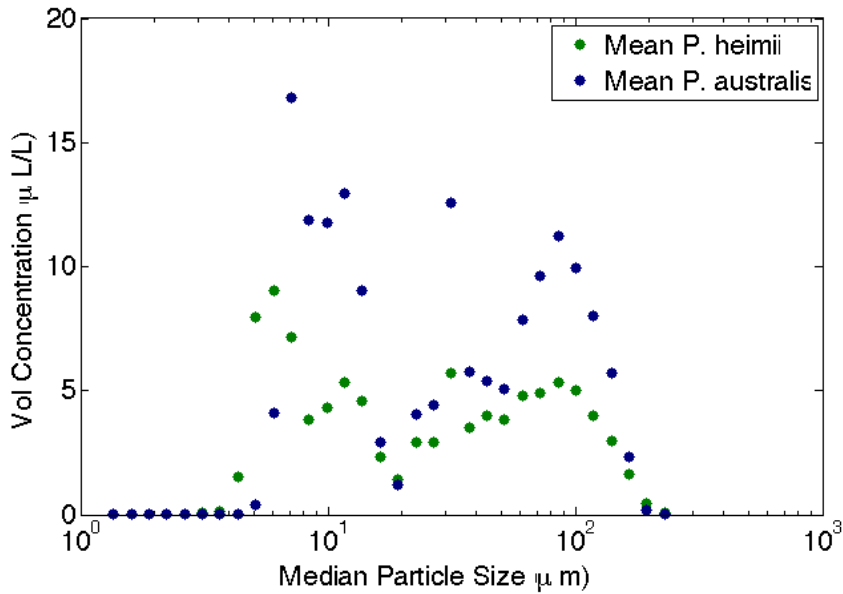
Figure 39. Mean *P. heimii* and *P. australis* PSD for 5,4, and 3-day monoculture tests. The data are an average of six experiments for each species, with different cell densities in each experiment. The data are averaged to determine organism signature from multiple experiments. The approximate cell widths and lengths for *P. heimii* and *P. australis* are 3-5 μm and 3-8 μm, and 30-100 μm and 50-100 μm, respectively.
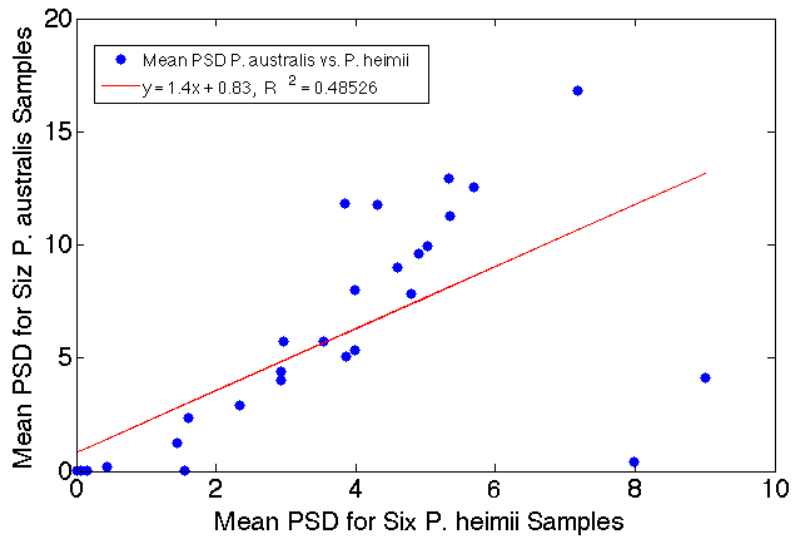
Figure 40. Scatter plot of mean PSD signatures for *P. australis* vs. *P. heimii*. To quantify the relationship between the mean PSD values for both species of *Pseudo-nitzschia* the values from Fig. 39 were scattered against each other and determined the weak linear relationship of y = 1.4x + 0.83, R^2=0.4. A linear regression analysis indicates a significant linear relationship between *P. heimii* and *P. australis*, $p < 0.001$, $[F(30.1) = 28.3]$.

4. Discussion

This research was driven by my desire to better understand how optical instruments mounted on an autonomous platform can describe plankton community composition. The motivation for this research was to optimize data collection and analysis of phytoplankton in the upper water column during an AUV deployment. The three questions I asked in this research were addressed by the three major sections of my thesis. In the first section I investigated the ability of the LISST-100X particle size distribution data to reconstruct fluorometer data using the MBARI May 2012 CANON data collected by the *Dorado* AUV. I conclude that combinations of the different size classes effectively reconstruct vehicle data, and that the combinations vary with the mean fluorescence values. In the second section I investigated the relationship between laboratory instrument counts of cell density and optical backscattering data for chlorophyll concentration by testing monocultures of phytoplankton on the ECO puck sensor. The results quantify the relationship between cell density and chlorophyll concentration for four monocultures of phytoplankton, and show different chlorophyll concentration per cell relationships for different sizes of phytoplankton. In the third section of this research I determined relationships between particle scattering distributions on the LISST-100X and phytoplankton species using monocultures. The LISST-100X gave different organism signatures for the small spherical, and unicellular monocultures as compared to the larger sized, pennate, chain-forming monocultures.

4.1 Optical Sensor Relationships: *In Situ* PSD and Fluorescence

Each section of this research investigated the relationships between multiple optical sensors mounted on AUVs that sample continuously to describe various aspects of the marine environment. The first section was part of a larger team effort to better understand the ability of the LISST-100X to describe upper water column composition using *in situ* data for particle scattering distribution and fluorescence. My work on that project included work with a Matlab program developed by Dr. Jim Bellingham that used LISST-100X PSD data to construct a surrogate for fluorescence data with the least residual error. The PSD surrogate consisted of a combination of six of the thirty-two logarithmically-spaced LISST-100X channels for particle sizes between 1.25 and 250 μm. With the code I developed in addition to the reconstruction algorithm, I analyzed data for two May 2012 CANON deployments of the *Dorado* AUV. Within those 12 and 14-hour datasets I chose subsets to determine whether the dominant particle size changed with fluorescence intensity. I split the continuous fluorescence and PSD data into subsets by time based upon a visual inspection of the full dataset for periods of high and low fluorescence.

For the full dataset and each of the three subsets I plotted the fluorescence signal against the PSD reconstruction and applied a linear regression to determine how well the PSD data replicate fluorescence. Those analyses resulted in eight scatter plots total; for each *Dorado* mission a full dataset analysis and three subplots based upon time periods of high and low fluorescence. In all but two of the eight regressions the R^2 values were approximately 0.6 or higher, indicating the linear fit for each data set described at least

60% of the data. The two plots of fluorescence vs. PSD that showed no linear

relationship were from periods of low fluorescence, sampled overnight (Table 3), and

supplied relatively few data points for the reconstruction analysis. For periods of high

fluorescence, between approximately 5E-4 and 6E-3 fluorescence units, channel 20

dominated the reconstruction values in all but one subset (*Dorado* 151, subset 1) where

channel 14 dominated the reconstruction (Table 3).

These results show that during periods of high and low fluorescence, different

particle sizes dominate the particle scattering distribution, suggesting that the PSD data

are detecting different fluorescing organisms with different levels of fluorescence. I

performed these analyses in Matlab using two sets of vehicle data from *Dorado* 150 (May

29-30, 2012) and *Dorado* 151 (May 30-31, 2012). Based upon the variability in

fluorescence intensities with time between the two *Dorado* datasets, I chose to group the

data by changes in persistent fluorescence values with time rather than generating subsets

for the same time periods each day. Further analysis could include a seasonal

comparison of *Dorado* fluorescence and PSD reconstruction data for subsets based upon

periods of high and low fluorescence. Analysis of data across multiple CANON missions

could give insight into changes in community composition with season, and if data sets

from multiple years are available, interannual variability in the particle scattering

distribution as it relates to community composition. Another benefit of analyzing

CANON data is the potential for comparison to other data collected during the mission,

which could give insight from processed water samples for community composition. An

example of this would be a comparison of the continuous fluorescence and PSD data

against the discrete gulper samples, 2L water samples taken *in situ* and processed in the lab. Such information could further support the results of the first section of my research, which showed the ability of a forward scattering particle size sensor to describe fluorescence in the coastal environment.

4.2 Optical Backscatter Sensor: ECO Puck

The second section of my research assessed the relationships between an optical backscatter oceanographic sensor and laboratory instruments using monocultures of phytoplankton. The goal for this section and the next were to determine the extent to which multiple optical sensors could identify and describe certain species of phytoplankton. The species in this study were chosen for their size and morphology differences. *Micromonas sp.* was chosen to represent the smallest end of the LISST-100X size class spectrum, and because the cells could be counted using a flow cytometer. The remaining three species were chosen because they are harmful algal bloom species. *Heterosigma akashiwo* is an ichthyotoxic red tide species that blocks fish gills at elevated concentrations (Frederickson, et al., 2011). A study of a *H. akashiwo* bloom in the Red Sea detected levels toxic to the brine shrimp *Artemia salina* (Mohamed & Al-Sheheri, 2012). *Pseudo-nitzschia heimii* and *Pseudo-nitzschia australis* are diatoms commonly found in Monterey Bay that, under certain conditions, are known to produce the neurotoxin domoic acid, which is implicit in amnesic shellfish poisoning (Fryxell, et al., 1997).

The tests performed using algal monocultures and the ECO puck backscatter sensor show a linear relationship between chlorophyll and cell density. The smaller (< 5 µm) organisms tested included *Micormonas sp.* and *Ostreococcus sp.*, and were both enumerated on a flow cytometer. The larger organisms included *Heterosigma akashiwo*, *P. heimii*, and *P. australis*, and were counted and measured using a Sedgewick rafter and microscopy. The relationship between chlorophyll concentration and cell density is two to three orders of magnitude larger for the three larger cell groups than for *Micromonas* (Table 5).

4.3 Forward Scattering Sensor: LISST-100X

The third section of this research investigated the organism signatures of the four species of phytoplankton discussed in section 2, on the LISST-100X forward scattering sensor. The results from the laboratory experiments and analysis showed distinct particle scattering distributions for each of the three genera tested, *Micromonas*, *Heterosigma*, and *Pseudo-nitzschia* (Figs. 29-36). The two species of *Pseudo-nitzschia* tested were similar in size and shape, both pennate and chain forming, though the *P. heimii* cells were slightly shorter and thinner than the *P. australis* cells (Table 1). The volume concentration distributions showed an increase with increasing concentration of monoculture in all four monoculture experiments (Figs. 29-36). The scattering signatures for the *Pseudo-nitzschia* cultures (Figs. 33 and 35) are consistent with the findings of Rienecker, et al (2008), that show a peak for the major (length) and minor (width) axes for the particle scattering distribution.

Further investigation into this organism signature identification study could include mixed samples of two or three different genera with known organism signatures. Experiments performed in Rienecker, et al. (2008) show that monocultures of different morphologies have unique organism signatures in tests of mixed cultures. In this project, a mixed experiment was performed using equal quantities of two monocultures of the same genus, *Pseudo-nitzschia*, to determine whether individual monocultures could be observed in the size distribution plot. The organism signatures for the two species from the same genus were too similar to clearly see different peaks in the mixed culture experiment. A mixed culture with *Micromonas* and *Heterosigma*, and *P. australis* tested on the LISST-100X could yield interesting results, as each has a unique organism signature when tested as monocultures. While the peak of *P. australis* associated with cell width (5-10 μm, Fig. 35) and the peak for *Heterosigma* (10-20 μm, Fig. 31) may be difficult to distinguish, the shape of the peaks were unique enough in the monoculture experiment that they should be clearly distinguished in a mixed culture experiment. The different genera tests in this project were performed at different times, so overlap in cell culturing with all three monocultures was not an option.

4.4 Applications

The research conducted in this project would not have been possible without the infrastructure, previous work, and support of the engineers and scientists of the autonomous underwater vehicle labs at MBARI and the MBARI summer internship program. The first section of this project was performed in the summer of 2012 with the

support of the Drew Gashler internship and under the mentorship of Dr. Bellingham in the LRAUV lab. The second and third sections of this research were conducted in summer 2013 and fall 2013. The monoculture cultivation, laboratory enumeration, and size determination of *Micromonas* and *Heterosigma* in summer 2013 were conducted in the Worden Lab with the guidance of Dr. Sebastian Sudek. The cultivation, microscopy enumeration, and size determination of both *Pseudo-nitzschia* cultures were performed in fall 2013 and early spring 2014 in the Scholin Lab with the guidance of Dr. Holly Bowers. Members of the AUV groups at MBARI, including John Ryan, Thomas Hoover, Denis Klimov, and Hans Thomas, provided critical assistance in laboratory set-up and sensor calibration. This research fits into the larger context of plankton community structure and optical sensor data analysis for autonomous sampling platforms.

Developing and conducting an interdisciplinary project comes with unique challenges and questions. One challenge included narrowing the scope of my proposed research questions. In this project I addressed my first three questions listed in section 1.4, but chose to keep question 4 to discuss potential future research and applications. The fourth question, which asked how definitively organism signatures determined from laboratory tests describe a phytoplankton population or bloom event from *in situ* data, was not addressed within the scope of this Masters thesis project. I asked the question, along with the other three questions I addressed, to consider applications of my work using *in situ* data. To address the question, however, requires time and resources outside of the scope of this project. The results from sections 1-3 of this research suggest that laboratory-determined organism signatures could be detected from *in situ* data, as the

Pseudo-nitzschia samples showed a consistent signature across the six tests performed (Figs. 37 and 38). Previous work in Rienecker, et al. (2008) also supports this idea, as that study found similar PSD signatures for *Pseudo-nitzschia* in the laboratory and *in situ* bloom events.

This project focuses on the ability of multiple instruments to describe phytoplankton *in situ*, particularly on an autonomous platform. An important motivation for this project came from the opportunity to work with sensor data from high-tech platforms for collecting data. AUVs provide tremendous insight through their ability to sample adaptively during a mission, and provide continuous data on ocean water conditions. These incredible tools for informing ocean processes and community composition are capable of identifying monocultures and can distinguish between different size classes and different cell shapes. That information is useful in identifying the morphologies of dominant characters in plankton bloom events. The particle size reconstruction of fluorometer data is useful in identifying the dominant size classes of chlorophyll-producing organisms with time and space, providing further insight into the sizes and shapes of plankton found *in situ*. There is real value in having that information with oceanographic sensors for O_2, tempearture, salinity, nitrate, photosynthetically active radiation, and others, in terms of the potential applications for harmful algal bloom prediction. Organism signatures and particle size reconstruction data plotted with nutrient and ocean condition data could give insight to bio-physical coupling during periods of high fluorescence or specific class size dominance, which in turn could yield indicators of optimal bloom conditions.   Through better understanding of the data

relationships between optical sensors mounted on AUVs, this research improves

characterization of upper water column communities by enhancing the ability to detect

and distinguish phytoplankton populations *in situ*.

References

Agrawal, Y.C. & H.C. Pottsmith. (2000). Instruments for particle size settling velocity observations in sediment transport. *Marine Geology*, 168:. 89-114.

Barlow, R.G., Mantoura, R.F.C., Gough, M.A., & Fileman, T.W. (1993). Pigment signatures of the phytoplankton composition in the northeastern Atlantic during the 1990 spring bloom. *Deep Sea Research Part II: Topical Studies in Oceanography*, 40(1–2): 459–477.

Bellingham, J.G., Hobson, B., Godin, M. A., Kieft, B., Erikson, J., McEwen, R., ... Mellinger, E. (2010) "A Small, Long-Range AUV with Flexible Speed and Payload," *Ocean Sciences Meeting*, Abstract MT15A-14, Portland, OR

Bowers, H.A., Tomas, C., Tengs, T., Kempton, J.W., Lewitus, A.J., & Oldach, D.W. (2006). Raphidophyceae (Chadefaud ex Silva) systematics and rapid identification: sequence analyses and real-time PCR assays. *Journal of Phycology 42*: 1333-1348.

Carroll, D. (2009). Carmel Bay: Oceanography dynamics and nutrient transport in a small embayment of the Central California Coast (Masters thesis). Moss Landing Marine Laboratories, Moss Landing, CA.

Cetinić, I., Toro-Farmer, G., Ragan, M., Oberg, C., & Jones, B. H. (2009). Calibration procedure for Slocum glider deployed optical instruments. *Optics Express*, *17*(18): 15420-15430.

Cheriton, O., McPhee-Shaw, E.E., Shaw, W.J., Stanton, T.P., Bellingham, J.G., & Storlazzi, C.D. (2013). Suspended particulate layers and internal waves over the southern Monterey Bay shelf: An important control on shelf mud belts? *Journal of Geophysical Research, 119*(1), 428-444. DOI: 10.1002/2013JC009360

Corlett, L. (1953). Net phytoplankton at Ocean Weather Stations "I" and "J". *J.Cons.int.Explor.Mer*. 19: 178-190.

Countway, P.D., & Caron, D.A. (2006). Abundance and distribution of *Ostreococcus sp.* in the San Pedro Channel, CA, as revealed by quantitative PCR. *Applied and Environmental Microbiology 72(*4), 2496-2506. DOI: 10.1128/AEM.72.4.2496-2506.2006

Das, J, Py, F., Maughan, T., O'Reilly, T., Messié, M., Ryan, ... Rajan, K. (2012). Coordinated sampling of dynamic oceanographic features with underwater vehicles and drifters. *The International Journal of Robotics Research 31*, 626-646.

Deerinck, T., Terada, M., Obiyashi, J., Ellisman. M., & Worden, A.Z. (2009). [Transmission electron microscope image of *Micromonas sp.*, 9 April 2009]. *Genes from tiny marine algae suggest unsuspected avenues for research*. Retrieved from http://www.mbari.org/news/news_releases/2009/micromonas/micromonas.html

Felip, M., & Catalan, J. (2000). The relationship between phytoplankton biovolume and chlorophyll in a deep oligotrophic lake: decoupling in their spatial and temporal maxima. *Journal of Plankton Research 22*(1), 91-105.

Frederickson, K.A., Strom, S.L., Crim, R., & Coyne, K.J. (2011). Interstrain variability in physiology and genetics of *Heterosigma akashiwo* (Raphidophyceae) from the West Coast of North America. *Journal of Phycology 47*, 25–35.

Fryxell, GA., Villac, M.C., & Shapiro, L.P. (1997). The occurrence of the toxic diatom species *Pseudo-nitzschia* (Bacillariophyceae) on the West Coast of the USA, 1920-1996: a review. *Phycologia, 36,* 419-437.

Gartner, J.W., Cheng, R.T., Wang, P.F., & Richter, K. (2001). Laboratory and field evaluations of the LISST-100 instrument for suspended particle size determinations. *Marine Geology*, *175*, 199-219.

Genty, B., Briantais, J., & Baker, N. (1989). The relationship between the quantum yield of photosynthetic electron transport and quenching of chlorophyll fluorescence. *BBA General Subjects, 990(1)*, 87-92.

Guillard, R.R.L. (1975). Culture of phytoplankton for feeding marine invertebrates. pp 26-60. In Smith W.L., & Chanley M.H (Eds.) *Culture of Marine Invertebrate Animals*. New York: Plenum Press.

Guillard, R.R.L., & Ryther, J.H. (1962). Studies of marine planktonic diatoms. I. *Cyclotella nana* Hustedt and *Detonula confervacea* Cleve. *Canadian Journal of Microbiology 8*: 229-239.

Guiry, M.D. (2013). *Heterosigma akashiwo* (Y.Hada) Y.Hada ex Y.Hara & M.Chihara, 1987. In: Guiry, M.D. & Guiry, G.M. (2013). AlgaeBase. World-wide electronic publication, National University of Ireland, Galway (taxonomic information republished from AlgaeBase with permission of M.D. Guiry). Accessed through: World Register of Marine Species at http://www.marinespecies.org/aphia.php?

HydroScat-2 Spectral Backscattering Sensor and Fluorometer User Manual, Revision 1. (2011). *HydroScat-2*. HOBI Labs, Bellvue, Washington. Instrument operated by the Monterey Bay Aquarium Research Institute.

Lynch, J.F., Irish, J.D., Sherwood, C.R., & Agrawal, Y.C. (1994). Determining suspended sediment particle size information from acoustical and optical backscatter measurements. *Continental Shelf Research 12*(10/11), 1139-1165.

McPhee-Shaw, E., & Kunze, E. (2002). Boundary layer intrusions from a sloping bottom: A mechanism for generating intermediate nepheloid layers. *Journal of Geophysical Research*,*107*(C6), 3-1—3-16. DOI: 10.1029/2001JC000801

Miller, C., & Wheeler, P. (2012). *Biological Oceanography*. Hoboken, NJ: Wiley.

Mohamed, Z. A., & Al-Sheheri, A.M. (2012). The link between shrimp farm runoff and blooms of toxic *Heterosigma akashiwo* in Red Sea coastal waters. *Oceanologia, 54*(2), 287–309.

Novak, T. (2011). Nitrate Transport to Coastal Monterey Bay: Investigating source inputs from Elkhorn Slough (Master's thesis). Moss Landing Marine Laboratories, Moss Landing, CA.

Pennington, J. T., & Chavez, F. P. (2000). Seasonal fluctuations of temperature, salinity, nitrate, chlorophyll and primary production at station H3/M1 over 1989–1996 in Monterey Bay, California. *Deep Sea Research Part II: Topical Studies in Oceanography*, *47*(5–6), 947–973.

Perry, M.J., & Porter, S.M. (1989). Determination of the cross-section absorption coefficient of individual phytoplankton cells by analytical flow cytometry. *Limnology and Oceanography, 34*, 1727-1738.

Rienecker, E., Ryan, J., Blum, M., Dietz, C., Coletti, L., Marin III, R., & Bissett, W.P. (2008). Mapping phytoplankton in situ using a laser-scattering sensor. *Limnology and Oceanography: Methods 6*, 153–161.

Ryan, J. P., McManus, M. A., Paduan, J. D., & F. P. Chavez. (2008). Phytoplankton thin layers caused by shear in frontal zones of a coastal upwelling system. *Marine Ecology Progress Series, 354*: 21–34.

Ryan, J.P., Johnson, S. B., Sherman, A., Rajan, K., Py, F., Thomas, H., ... Vrijenhoek, R. C. (2010). Mobile autonomous process sampling within coastal ocean observing systems. *Limnology and Oceanography: Methods*, *8*: 394–402.

Ryan, J.P., McManus, M.A., Kudela, R.M., Lara Artigas, M., Bellingham, J.G., Chavez, F.P., ... Zhang, Y. (2013). Boundary influences on HAB phytoplankton ecology in a stratification-enhanced upwelling shadow. *Deep Sea Research Part II*: *Topical Studies in Oceanography*.

Sieburth, J. M., Smetacek, V., & Lenz, J. (1978). Pelagic ecosystem structure: Heterotrophic compartments of the plankton and their relationship to plankton size fractions. *Limnology and Oceanogr*aphy, *23*: 1256-1263.

Skogsberg, T. (1936). Hydrography of Monterey Bay, California. Thermal conditions, 1929–1933. *Transactions of the American Philosophical Society*, 29: 1–152.

Skogsberg, T., & Phelps, A. (1946). Hydrography of Monterey Bay, California. Thermal conditions, Part II, 1934–1937. *Proceedings of the American Philosophical Society*, *90*, 350–386.

Suggett, D.J., Moore, C.M., & Geider, R.J. (2011). Estimating Aquatic Productivity from Active Fluorescence Measurements. In *Chlorophyll* a *Fluorescence in Aquatic Sciences: Methods and Applications,* D.J. Suggett, O. Prasil, & M.A. Borowitzka, Eds. pp. 103-127. Springer Science + Business Media.

Worden, A. Z., & Not, F. (2008). Ecology and Diversity of Picoeukaryotes. In *Microbial Ecology of the Oceans,* D. L. Kirchman, Ed. (pp. 159–205). Hoboken, NJ: Wiley.

Woodson, C.B., Washburn, L., Barth, J.A., Hoover, D.J., Kirincich, A.R., McManus, M.A., ... Tyburczy, J. (2009). Northern Monterey Bay upwelling shadow front: Observations of a coastally and surface-trapped buoyant plume. *Journal of Geophysical Research, 114.*

Stratton, J. A. (1941). *Electromagnetic Theory*. New York: McGraw-Hill.

Thomas, C.R. (1997). *Identifying Marine Phytoplankton*. San Diego: Academic Press.

Zhang, Y., McEwen, R. S., Ryan, J. P., Bellingham, J. G. (2009). An Adaptive Triggering Method for Capturing Peak Samples in a Thin Phytoplankton Layer by an Autonomous Underwater Vehicle. *Proceedings of MTS/IEEE Oceans'09.* Biloxi, Mississippi, U.S.A. pp. 1-5.